Mon. Not. R. Astron. Soc. **359,** 1165–1183 (2005) doi:10.1111/j.1365-2966.2005.08979.x

# An interferometric CO survey of luminous submillimetre galaxies

T. R. Greve,[1,2★] F. Bertoldi,[3] Ian Smail,[4] R. Neri,[5] S. C. Chapman,[2] A. W. Blain,[2] R. J. Ivison,[1,6] R. Genzel,[7,8] A. Omont,[9] P. Cox,[10] L. Tacconi[7] and J.-P. Kneib[2,11,12]

[1]*Institute for Astronomy, University of Edinburgh, Blackford Hill, Edinburgh EH9 3HJ*
[2]*California Institute of Technology, Pasadena, CA 91125, USA*
[3]*Max-Planck Institut für Radioastronomie(MPIfR), Bonn, Germany*
[4]*Institute for Computational Cosmology, University of Durham, South Road, Durham DH1 3LE*
[5]*Institut de Radio Astronomie Millimétrique (IRAM), St Martin d'Hères, France*
[6]*Astronomy Technology Centre, Royal Observatory, Blackford Hill, Edinburgh EH9 3HJ*
[7]*Max-Planck Institut für extraterrestrische Physik (MPE), Garching, Germany*
[8]*Department of Physics, University of California, Berkeley, USA*
[9]*Institut d'Astrophysique de Paris, CNRS, Université de Paris, Paris, France*
[10]*Institut d'Astrophysique Spatiale, Université de Paris Sud, Orsay, France*
[11]*Observatoire Midi-Pyrénées, UMR5572, 14 Avenue Edouard Belin, 31400 Toulouse, France*
[12]*Laboratoire d'Astrophysique de Marseille, UMR 6110, CNRS-Université de Provence, Traverse du Siphon-Les trois Lucs, 13012 Marseille, France*

Accepted 2005 February 28. Received 2005 February 25; in original form 2004 October 13

**ABSTRACT**

In this paper, we present results from an Institut de Radio Astronomie Millimétrique (IRAM) Plateau de Bure millimetre-wave Interferometer (PdBI) survey for carbon monoxide (CO) emission towards radio-detected submillimetre galaxies (SMGs) with known optical and near-infrared spectroscopic redshifts. Five sources in the redshift range $z \sim 1$–3.5 were detected, nearly doubling the number of SMGs detected in CO. We summarize the properties of all 12 CO-detected SMGs, as well as six sources not detected in CO by our survey, and use this sample to explore the bulk physical properties of the submillimetre galaxy (SMG) population as a whole. The median CO line luminosity of the SMGs is $\langle L'_{\rm CO}\rangle = (3.8 \pm 2.0) \times 10^{10}\,{\rm K\,km\,s^{-1}\,pc^2}$. Using a CO-to-$H_2$ conversion factor appropriate for starburst galaxies, this corresponds to a molecular gas mass $\langle M({\rm H_2})\rangle = (3.0 \pm 1.6) \times 10^{10}\,{\rm M_\odot}$ within an $\sim 2$ kpc radius, approximately 4 times greater than the most luminous local ultraluminous infrared galaxies (ULIRGs) but comparable to that of the most extreme high-redshift radio galaxies (HzRGs) and quasi-sellar objects (QSOs). The median CO FWHM linewidth is broad, $\langle {\rm FWHM}\rangle = 780 \pm 320\,{\rm km\,s^{-1}}$, and the SMGs often have double-peaked line profiles, indicative of either a merger or a disc. From their median gas reservoirs ($\sim 3 \times 10^{10}\,{\rm M_\odot}$) and star formation rates ($\gtrsim 700\,{\rm M_\odot\,yr^{-1}}$), we estimate a lower limit on the typical gas-depletion time-scale of $\gtrsim 40$ Myr in SMGs. This is marginally below the typical age expected for the starbursts in SMGs and suggests that negative feedback processes may play an important role in prolonging the gas consumption time-scale. We find a statistically significant correlation between the far-infrared and CO luminosities of the SMGs, which extends the observed correlation for local ULIRGs to higher luminosities and higher redshifts. The non-linear nature of the correlation implies that SMGs have higher far-infrared to CO luminosity ratios and possibly higher star formation efficiencies (SFEs), than local ULIRGs. Assuming a typical CO source diameter of $\theta \sim 0.5$ arcsec ($D \sim 4$ kpc), we estimate a median dynamical mass of $\langle M_{\rm dyn}\rangle \simeq (1.2 \pm 1.5) \times 10^{11}\,{\rm M_\odot}$ for the SMG sample. Both the total gas and stellar masses imply that SMGs are very massive systems, dominated by baryons in their central regions. The baryonic and dynamical properties of these systems mirror those of local giant ellipticals and are consistent with numerical simulations of the formation of the most massive galaxies. We have been able to impose a lower limit of $\gtrsim 5 \times 10^{-6}\,{\rm Mpc^{-3}}$ to the comoving number density of massive galaxies in the redshift range

★E-mail: tgreve@submm.caltech.edu

$z \sim 2$–3.5, which is in agreement with results from recent spectroscopic surveys and the most recent model predictions.

**Key words:** galaxies: formation – galaxies: starburst – cosmology: observations – early Universe.

## 1 INTRODUCTION

The discovery of extragalactic carbon monoxide (CO) rotational line emission (Rickard et al. 1975) and, in particular, the first detections of CO at cosmologically significant redshifts in IRAS F10214+4724 at $z = 2.29$ (Brown & Vanden Bout 1991; Solomon, Downes & Radford 1992a), the Cloverleaf at $z = 2.56$ (Barvainis et al. 1994) and BRI 1202−0725 at $z = 4.69$ (Omont et al. 1996) revealed the potential of CO as a tracer of molecular gas in the early Universe. Since those pioneering efforts, progress has been slow as a result of the severe observational obstacles: the faintness of the CO emission, except for cases were the source is gravitationally magnified; inaccurate spectroscopic redshifts coupled with the small instantaneous bandwidth of most modern-day correlators; and in some cases, an unfortunate combination of redshift and available receiver coverage, as well as atmospheric transparency, at millimetre wavelengths. As a result, only 30 or so $z > 1$ objects have been detected to date, most of which have been extremely luminous, often gravitationally lensed, quasi-sellar objects (QSOs; e.g. Omont et al. 1996; Guilloteau et al. 1997; Downes et al. 1999; Guilloteau et al. 1999; Cox et al. 2002; Bertoldi et al. 2003; Beelen et al. 2004) and high-redshift radio galaxies (HzRGs; e.g. Papadopoulos et al. 2000; De Breuck et al. 2003a).

The slow increase in the number of CO detections contrasts with the rapid growth in samples of high-redshift galaxies selected through continuum observations at submillimetre (submm) wavelengths, which detect thermal emission from dust. The advent of large-format submm/mm cameras, the Submillimetre Common-User Bolometer Array (SCUBA) (Holland et al. 1999) and the Max-Planck Millimeter Bolometer (MAMBO) (Kreysa et al. 1998), revealed the presence of a significant population of dust-enshrouded and therefore hitherto undetected galaxies at high redshifts (e.g. Smail, Ivison & Blain 1997; Barger, Cowie & Sanders 1999; Bertoldi et al. 2000). Today such observations are routine and several hundred submm-selected (or SCUBA) galaxies (SMGs) have been discovered (e.g. Blain et al. 2002; Scott et al. 2002; Borys et al. 2003; Webb et al. 2003).

Until recently, only two SMGs had been detected in CO (Frayer et al. 1998, 1999; Downes & Solomon 2003; Genzel et al. 2003), largely owing to the extreme faintness of SMGs in the optical and the difficulties in obtaining reliably spectroscopic redshifts. However, a major step forward was made by Chapman et al. (2003b, 2005) who used the highly efficient, blue-sensitive Low-Resolution Imaging Spectrometer (LRIS)-B spectrograph on the Keck Telescope to obtain spectroscopic redshifts for a large sample of SMGs. This motivated a major survey at the Institut de Radio Astronomie Millimétrique (IRAM) Plateau de Bure Interferometer (PdBI) to look for CO emission from this high-redshift sample. The observational cycle involves: identifying a robust radio counterpart to a submillimetre galaxy (SMG) in deep Very Large Array (VLA) radio maps (see e.g. Ivison et al. 2002); placing an LRIS-B/Keck slit on this position to obtain a spectroscopic redshift (Chapman et al. 2003b, 2005); frequently confirming the redshift in the near-infrared, usually via redshifted H$\alpha$ (Simpson et al. 2004; Swinbank et al. 2004); and, finally, searching for redshifted CO emission with PdBI. The initial results from this CO programme were described in Neri et al. (2003). Although an expensive process in terms of telescope time, this is currently the only feasible and effective route for detecting CO from SMGs.

CO observations can potentially provide unique information about the enigmatic SMG population. First and foremost, CO traces the bulk of the molecular gas in SMGs: the high-level ($J \geqslant 2$) transitions arise in the warm and dense gas, while lower level $J$ lines probe the quiescent and likely cooler gas, which may lurk in the outskirts of SMGs. Detecting and mapping this molecular emission enables us to precisely determine the spatial and kinematic location of the gas-rich components within an SMG. About two-thirds of SMGs are found to be large, morphologically complex systems in the optical/near-infrared and/or the radio, with typically one or more companions (e.g. Smail et al. 1999; Ivison et al. 2002; Chapman et al. 2003c, 2004). For example, in one SMG, Neri et al. (2003) identified CO emission coincident with a second, fainter radio source $\sim 4$ arcsec away from the radio counterpart for which the spectroscopic redshift had been found. Secondly, CO observations yield fairly accurate estimates of the amount of molecular gas available to fuel the starburst and/or the AGN responsible for the large far-infrared luminosities. While the conversion factor between the CO luminosity and molecular gas mass is uncertain, CO observations clearly provide a much better constraint on the amount of gas present in SMGs than the estimates based on submm continuum observations and an adopted spectral energy distribution (SED) and gas-to-dust ratio.

The first two CO detections of SMGs revealed the presence of copious amount of molecular gas ($\sim 10^{10}\,\mathrm{M}_{\odot}$), suggesting that intense star formation is occurring in these systems (Frayer et al. 1998, 1999). Furthermore, from a reliable estimate of the gas reservoir in an SMG, we can say something about the gas exhaustion time-scale, i.e. the duration of the submm-luminous phase. This, in turn, allows us to make an educated guess about the possible descendants of SMGs, and thus place them in an evolutionary context with other high- and low-redshift galaxy populations.

Observations of the shape and width of CO lines also provides important information about the kinematics in SMGs (Neri et al. 2003; Tacconi et al. 2005). In particular, if the CO emission is spatially resolved we can use that, in conjunction with the width of the line profile, to constrain the dynamical mass of the host galaxy. Estimates of the dynamical mass based on CO are likely to be cleaner than estimates from optical/near-infrared spectroscopy, which are prone to extinction by dust and the effects of non-gravitational motions in the emitting gas, such as outflows. The best example of resolved CO emission in an SMG (Genzel et al. 2003) shows gas extended on scales of $\sim$3–5 kpc and that most of the dynamical mass ($\sim 3 \times 10^{11}\,\mathrm{M}_{\odot}$) is baryonic. Such large, widely distributed gas reservoirs suggest that the brightest SMGs are not merely

**Table 1.** Log of the Plateau de Bure millimetre-wave Interferometer (PdBI) observations for the 11 submillimetre galaxies (SMGs) analysed in this paper. The on-source integration time ($t_{\rm int}$) is the observing time for the equivalent six-element array.

| Source | Observing dates | $t_{\rm int}$ (hr) | Detection? |
|---|---|---|---|
| SMM J02396−0134 | 1999 Jun 20, 24–26, 29, Aug 24, 27, Sep 7 | 7.4 | Y |
| SMM J10523+5722 | 2003 Apr 25, May 06 | 16.6 | N |
| SMM J10524+5724 | 2003 Mar 27 | 3.9 | N |
| SMM J12360+6210 | 2003 Jun 01, 03, 18, Aug 30, Sep 01 | 9.4 | N |
| SMM J13120+4242 | 2003 May 17, 22–23, 26 | 9.2 | Y |
| SMM J13123+4239 | 2003 Jun 23, 26, 27 | 4.7 | N |
| SMM J16363+4055 | 2003 Mar 31, Apr 03, 21 | 11.2 | N |
| SMM J16363+4056 | 2003 Aug 11, 22, 24 | 9.6 | N |
| SMM J16366+4105 | 2003 Apr 13–14, 23, May 1 | 14.9 | Y |
| SMM J16371+4053 | 2003 Jul 25–26, 29 Aug 1,2, Sep 4 | 17.1 | Y |
| SMM J22174+0015 | 2003 May 9–13, 29–30, Jun 4, Sep 12, 14 | 17.3 | Y |

high-redshift replicas of the local population of ultraluminous infrared galaxies (ULIRGs). However, a representative picture of the gas distribution in SMGs will have to await high-resolution CO observations of a large sample of SMGs.

Because CO observations provide a means of weighing galaxies at high redshifts, both in terms of their baryonic gas mass content and their total dynamical mass, they can be used to help piece together a picture of the mass assembly of massive galaxies in the early Universe. In the classical cold dark matter (CDM) scenario of structure formation (White & Frenk 1991), massive spheroidal galaxies are the end products of a gradual build-up of mass via merging and, as a result, form late in the history of the Universe. However, as pointed out by Genzel et al. (2003), at least some SMGs appear to be massive, baryon-dominated galaxies already at $z \sim 2$–3. The discovery of massive, evolved early-type galaxies at $z \gtrsim 1.5$ (e.g. Cimatti et al. 2004), which could be the descendants of $z \gtrsim 2$ SMGs, suggests that some massive spheroids were not formed at $z \lesssim 1$. In fact, if the brightest 25 per cent of the SMGs are massive baryonic systems, then their abundance indicates that the build-up of massive galaxies in the early Universe was much faster than previously expected and could pose a serious challenge for current models of gas processing in galaxy formation (e.g. Cole et al. 1994; Kauffmann et al. 1999; Baugh et al. 2005).

In this paper, we present the most recent results from a systematic survey of CO emission towards radio-identified SMGs with spectroscopic redshifts in the range $z \sim 1$–3.5 (corresponding to 40–10 per cent of the age of the Universe at the respective epochs) and use these to address the issues outlined above. This is part of a major effort currently being undertaken at the PdBI with the aim of detecting and imaging CO emission towards $\sim$20–30 SMGs. In Sections 2 and 3, we describe the observations and derive properties for each new source observed. In Section 4, we define a sample of 12 sources consisting of all SMGs detected in CO to date, from which the average physical properties of the bright SMG population are derived. We discuss their properties and compare with those of other galaxy populations in Section 5. Finally, Section 6 discusses the impact of our observations on models of galaxy formation and evolution. Throughout we adopt a flat cosmology, with $\Omega_{\rm m} = 0.27$, $\Omega_\Lambda = 0.73$ and $H_0 = 71\,{\rm km\,s^{-1}\,Mpc^{-1}}$ (Spergel et al. 2003).

## 2 OBSERVATIONS

In total, 11 SMGs were targeted for CO observations with PdBI (see Table 1), drawn from five independent submm surveys: the SCUBA Lens Survey (SMM J02396−0134, Smail et al. 1997); the *Hubble Deep Field* (SMM J12360+6210, Chapman et al. 2003a); the Hawaii Survey Fields, SSA 13 and SSA 22 (SMM J13120+4242, SMM J13123+4239, Chapman et al. 2005; SMM J22174+0015, Barger et al. 1999); the SCUBA UK 8-mJy Survey of the Lockman Hole East and ELAIS N2 (SMM J10523+5722, SMM J10524+5724, SMM J16363+4055, SMM J16363+4056 and SMM J16366+4105, Scott et al. 2002); and a 1200-μm MAMBO survey of the same two fields (SMM J16371+4053,[1] Greve et al. 2004b).

Deep radio imaging was used to identify radio counterparts to all the targeted SMGs and accurately locate these relative to optical/near-infrared reference fields (Smail et al. 1999; Ivison et al. 2002; Chapman et al. 2003a). Subsequent spectroscopy with Keck/LRIS-B (Oke et al. 1995) and Canada–France–Hawaii Telescope (CFHT) Optionally Stabilized Imager and Spectrometer (OSIS) in the case of SMM J02396−0134 (Soucail et al. 1999) provided ultraviolet (UV) spectroscopic redshifts for all sources (see Chapman et al. 2003b, 2005). A subset of the sample was spectroscopically observed in the near-infrared to provide more reliable systemic redshifts from the wavelengths of redshifted H$\alpha$ or [O III] $\lambda$5007 Å emission lines (Swinbank et al. 2004) to aid in our search for redshifted CO emission. Here and for the remainder of this paper, we take the systemic redshift to be equivalent to the CO redshift.

From our sample of 11 sources, 10 were part of our statistically complete CO survey and were targeted during two observing campaigns, during the winter of 2002–2003 and the summer of 2003, in good to excellent weather. The observations were done in D configuration in order to maximize the sensitivity and used five of the six available antennae, giving a total of 10 baselines. We stress that the survey is ongoing and that the 10 sources reported here are merely those that were observed during the 2003 season. In addition, we included an 11th source, SMM J02396−0134, for which data was originally obtained by J.-P. Kneib and G. Soucail during the summer/autumn of 1999, and these were retrieved from the PdBI data archive. Observations of this source were done in D and C configuration. The details of the observations of all 11 sources are summarized in Table 1.

While our main goal was to detect redshifted CO emission in the 3-mm waveband, we also used the 1.3-mm receivers to attempt to determine accurate continuum positions and fluxes or, in cases where a

[1] This source was denoted MM J16371+4053 in Greve et al. (2004b).

higher-$J$ CO line would coincide with the 1.3-mm band, to search for emission from this transition, e.g. SMM J04431+0210 (Neri et al. 2003). To achieve our goals the correlators were configured for line and continuum observations and simultaneously covered 580 MHz in the 3 and 1.3-mm bands: this corresponds to a typical velocity coverage of 1700 and 750 km s$^{-1}$ at 3 and 1.3 mm, respectively.

Where a near-infrared spectroscopic redshift was unavailable, we have to correct for the likely systematic blueshifts of UV line features relative to the CO emission. We therefore tuned the 3-mm receivers slightly redward of the measured spectroscopic redshift. This meant that for a typical redshift uncertainty of $\Delta z = 0.005$, any source at $z \geqslant 1$ would have its CO line peak fall within $0.5 \times 580$ MHz $=$ 290 MHz of the 3-mm-band centre. In a few instances, a line was detected at the edge of the bandpass. The frequency setting was then adjusted to centre the line in the bandpass and the source was re-observed. A source was typically observed for 2–3 tracks (10–18 h). If no signal had been detected after this, the source was not pursued further.

All data reduction employed the IRAM GILDAS software (Guilloteau & Lucas 2000). This involved careful monitoring of the quality of the data throughout a track, and subsequent flagging of any bad and high phase-noise visibilities. For passband calibration, we typically used one or more bright quasars. Phase and amplitude variations within each track were calibrated out by interleaving reference observations of nearby fainter quasars every 20 m. In the best conditions, the typical rms phase noise per baseline at 3 mm was $\lesssim 10^\circ$, increasing to $\lesssim 40^\circ$ in the worst cases. Observations of the primary calibrators, 3C 454.3, 3C 345, 3C 273 and MWC 349, were used to determine the flux scale. Finally, naturally weighted data cubes were created using GILDAS.

## 3 THE SOURCES

No sources were detected at 1.3 mm and the data were of such poor quality that even upper limits were useless. For the remainder of this paper, we shall therefore only discuss the 3-mm data. For each source, the continuum level at 3 mm was estimated by extrapolating from its submm flux and assuming a spectral index of $\beta = 1.5$. In all cases, we find the contribution from the continuum emission to the CO line at 3 mm to be less than $\lesssim 5$ per cent and therefore negligible. Of the 11 sources whose observations are analysed in this paper, CO emission was reliably detected in five. Including the first three (out of three) detections from our survey from Neri et al. (2003) yields a detection rate of 57 per cent (8/14) to date.

The failure to detect CO in some of our sources is unlikely to be the result of the optical redshift being wrong, because the quality of the spectra is generally high (Chapman et al. 2005). Similarly, the possibility that the identification is wrong and therefore the redshift is for the wrong object appears to be remote given the excellent correspondence between the radio and submm (e.g. Ivison et al. 2002), and the extremely small likelihood of finding a $z \sim 2$ galaxy at that position, which is not related to the submm emission. Instead, we feel the explanation for the missing CO emission is the result of either too large a velocity offset between the CO and optical emission (putting the former outside our selected correlator coverage, see Section 4.2), a CO line with a width comparable to our correlator bandwidth, or simply that the sources are too faint in CO to be detected in the given integration time. In the latter case, the six non-detections can provide useful upper limits on their CO luminosity and gas masses and as a result we have included them in the analysis in this paper.

In the remainder of this section, we shall briefly describe the properties of the five SMGs for which new CO detections are presented in this paper as well as the six non-detections.

### 3.1 SMM J02396−0134

The CO(2–1) spectrum of SMM J02396−0134 is shown in Fig. 1(a). The blue wing of the line is missing as a result of the limited correlator bandwidth available in 1999, but none the less it is evident that the line is double peaked. The CO redshift, $z_{\rm CO} = 1.062 \pm 0.002$, was defined as the flux-weighted redshift (see Section 4.2 for details). The widths of the two peaks were estimated by simultaneously fitting two Gaussians to the spectrum, which yielded FWHM values $180 \pm 20$ and $430 \pm 50$ km s$^{-1}$ for the blueshifted and redshifted peaks, respectively. The velocity offsets of the two peaks were $-280$ and 90 km s$^{-1}$, respectively, measured relative to the CO redshift. From the double Gaussian fit, the velocity-integrated CO(2–1) line flux is $I_{\rm CO} = 3.4 \pm 0.3$ Jy km s$^{-1}$. A single Gaussian fit to the line profile leads to a FWHM value of $780 \pm 60$ km s$^{-1}$. As a result of the truncated line, we can only impose a lower limit $\simeq 870$ km s$^{-1}$ on the full width at zero intensity (FWZI).

The emission integrated over the line from $-460$ to 110 km s$^{-1}$ is shown as contours overlaid on a $K$-band image in Fig. 2(a). The emission is detected at $\geqslant 10\sigma$, where $\sigma = 0.40$ mJy beam$^{-1}$, and coincides with the optical/near-infrared counterpart to within the relative astrometrical errors. The source appears extended in the north–south direction and an elliptical Gaussian fit to the CO emission in the image plane yields a source size of $9.5 \times 5.5$ arcsec, which is slightly larger than the $8.3 \times 5.3$ arcsec synthesized beam. The two velocity components of the source have a slight spatial offset, with the blueshifted peak (integrated from $-460$ to $-120$ km s$^{-1}$) 1.2 arcsec north of the centroid of the integrated line emission and the redshifted peak (integrated from $-120$ to 110 km s$^{-1}$) offset 0.3 arcsec east and 1.6 arcsec south of the central position. The positional uncertainties in the maps are 0.3–0.4 arcsec, suggesting that the observed offsets are significant.

### 3.2 SMM J13120+4242

The CO(4–3) spectrum of SMM J13120+4242 is shown in Fig. 1(e). A single Gaussian provides an excellent fit to the data, as measured by the $\chi^2$ statistic, and yields a velocity-integrated flux density, $1.7 \pm 0.3$ Jy km s$^{-1}$, and a linewidth of FWHM $\simeq 530 \pm 50$ km s$^{-1}$. We find a systemic CO redshift of $z_{\rm CO} = 3.408 \pm 0.002$.

The velocity-integrated CO(4–3) emission yields a $\gtrsim 6\sigma$ detection ($\sigma = 0.32$ mJy beam$^{-1}$) at a position that is offset 0.8 arcsec to the north-east of the optical counterpart (Fig. 2b). The positional error is $\sim 1$ arcsec and so the offset is not significant. The CO emission is unresolved.

### 3.3 SMM J16366+4105

The CO(3–2) spectrum of SMM J16366+4105 (Fig. 1i) is very broad with the blue edge of the line ending abruptly. The spectrum exhibits a double-peaked line similar to SMM 02396−0134, although less distinct. The CO redshift is $z = 2.450 \pm 0.002$. A simultaneous fit of two Gaussians provides a superior fit to the spectrum than does a single Gaussian, and places the blueshifted and redshifted peaks at velocity offsets of $-270$ and $+210$ km s$^{-1}$, respectively. The velocity-integrated line flux is $I_{\rm CO} = 1.8 \pm 0.3$ Jy km s$^{-1}$. A single Gaussian fitted to the spectrum yields a linewidth FWHM $=$ $870 \pm 80$ km s$^{-1}$: the second largest linewidth of the sample.

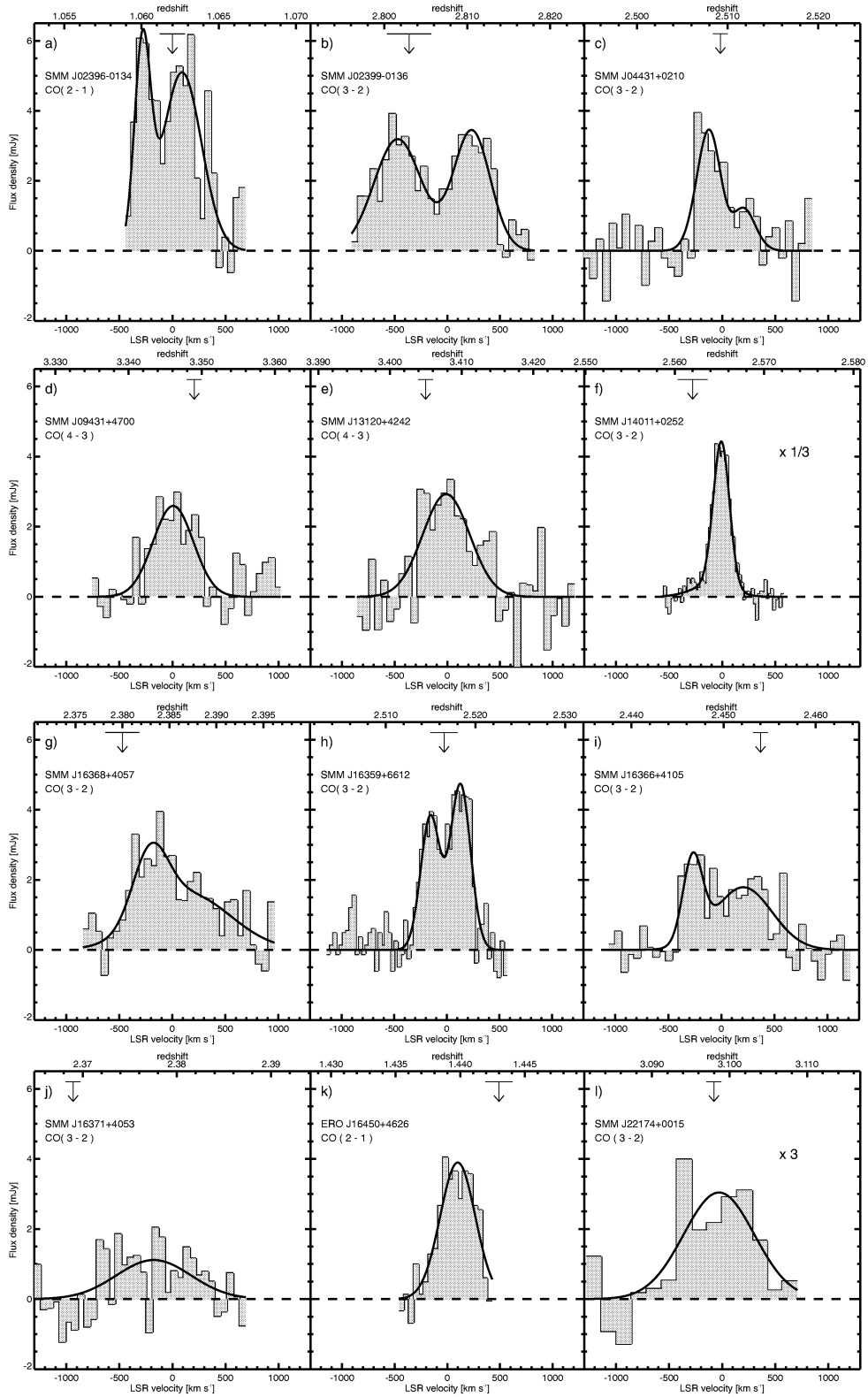


**Figure 1.** CO line profiles of the 12 submillimetre galaxies (SMGs) detected in CO to date. The profiles have been plotted on similar flux and velocity scales in order to facilitate an easy comparison between individual sources, to achieve this the spectra of SMM J14011+0252 and SMM J22174+0015 have been scaled by a factor of 1/3 and 3, respectively. The local standard of rest velocity scale is relative to the CO redshift. Optical redshifts are denoted by arrows and the horizontal bars on top of the arrows indicate the uncertainty of the redshifts. The redshifts derived from the CO lines are given in Table 2. The solid curves represent the best fits to the spectra using either single or double Gaussian profiles. The spectra shown in (c), (d) and (g) are taken from Neri et al. (2003); (h) is taken from Kneib et al. (2004), while (b), (f) and (k) are from Genzel et al. (2003), Downes & Solomon (2003) and Andreani et al. (2000), respectively. The spectra have been binned into 20 MHz bins, except for (f), (h) and (l) where the frequency binning is 7, 10 and 40 MHz, respectively.

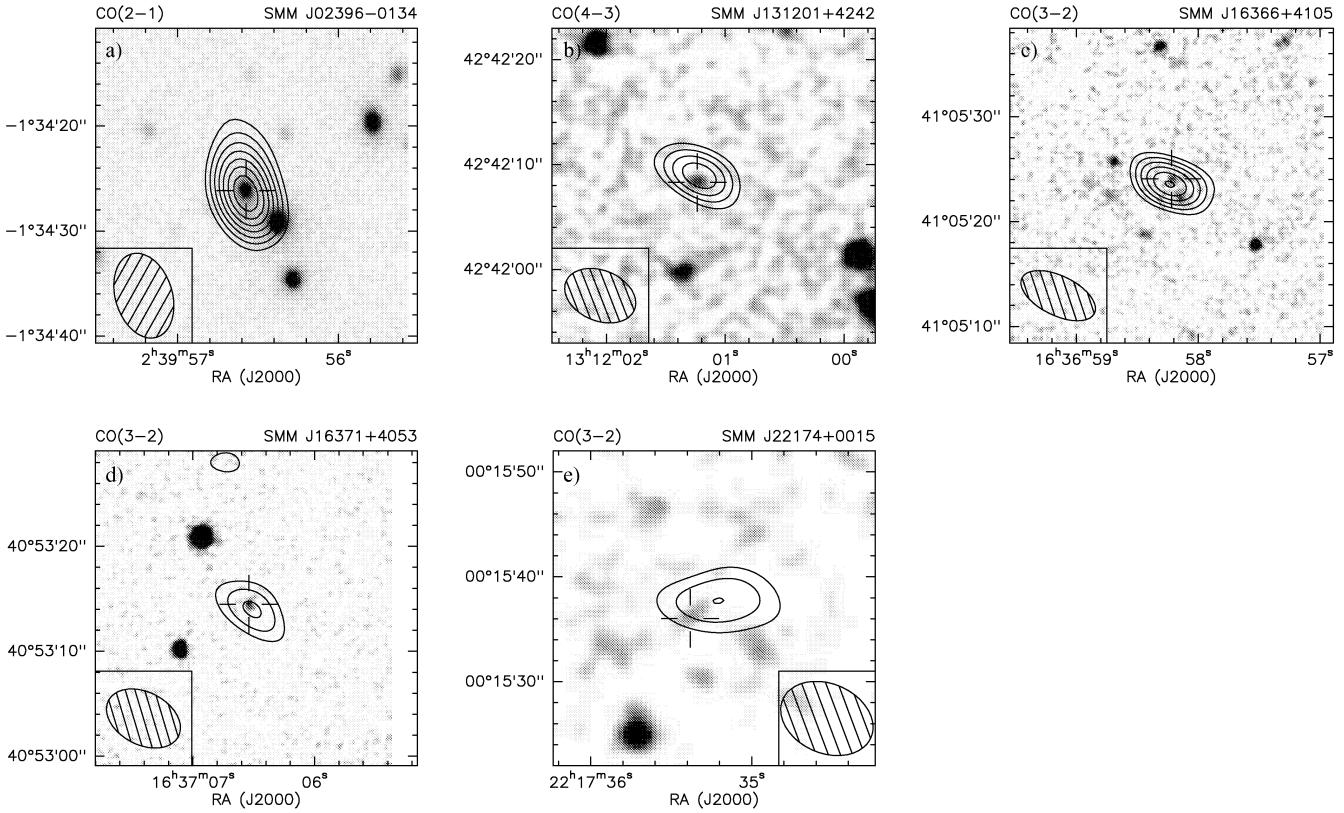


**Figure 2.** Contours of the velocity integrated CO emission overlaid on 30 × 30 arcsec $K$-band images of the five new CO-detected submillimetre galaxies (SMGs) presented in this paper. The $K$-band images are centred on the radio positions, while the open crosses mark the position of the optical/near-infrared counterparts for which the spectroscopic redshifts were obtained. In all panels, the contours start at $3\sigma$ and increase in steps of $1\sigma$, where $\sigma = 0.40, 0.32, 0.21, 0.18$ and $0.17\,\mathrm{mJy\,beam^{-1}}$ in panels (a), (b), (c), (d) and (e), respectively. The synthesized beams are (panels a to e, shown as hatched ellipses) 8.3 × 5.3 arcsec at position angle 15° (east of north), 6.9 × 4.8 arcsec at 66°, 7.4 × 3.9 arcsec at 62°, 7.4 × 5.0 arcsec at 61° and 9.0 × 6.6 arcsec at 65°. The ($1\sigma$) uncertainties on measured positions in the optical and mm frames are $\lesssim$0.1 and $\lesssim$0.3 arcsec, respectively. The $K$-band data for (a), (b) and (e) were published in Smail et al. (2002, 2004) and Chapman et al. (2003a), respectively, while (c) and (d) were published in Ivison et al. (2002).

The integrated CO emission, shown in Fig. 2(c), is detected at the $\gtrsim 8\sigma$ level ($\sigma = 0.21\,\mathrm{mJy\,beam^{-1}}$), and coincides with the radio and faint optical/near-infrared counterpart. We imaged the blueshifted and redshifted peaks separately, using different velocity cut-offs, in order to look for positional offsets between the two, but found no evidence for a velocity gradient across the source. It is possible that part of the CO emission is related to the faint near-infrared source $\sim 2$ arcsec south-west of the CO centroid, the compact radio counterpart displays a similar faint tail of emission in this direction. SMM J16366+4105 is a prime target for further, higher-resolution CO observations.

### 3.4 SMM J16371+4053

The detection of CO(3–2) towards SMM J16371+4053 is the first for a MAMBO-selected source. The CO(3–2) line profile is shown in Fig. 1(j). The flux-weighted, systemic CO redshift is $z_{\mathrm{CO}} = 2.380 \pm 0.004$. While clearly detected, the poor signal-to-noise ratio prevents us from defining the line profile, except to say that the line appears broad with FWZI $\gtrsim 900\,\mathrm{km\,s^{-1}}$. A Gaussian fit yields a formal linewidth of FWHM $\sim 830\,\mathrm{km\,s^{-1}}$ and a velocity-integrated line flux $I_{\mathrm{CO}} = 1.0 \pm 0.2\,\mathrm{Jy\,km\,s^{-1}}$.

The integrated emission is shown in Fig. 1(d). The source is detected at $\gtrsim 5\sigma$ ($\sigma = 0.18\,\mathrm{mJy\,beam^{-1}}$) and coincides with the optical/near-infrared counterpart to within the positional errors.

### 3.5 SMM J22174+0015

The CO(3–2) spectrum of this source shown in Fig. 1(l) is the weakest of our detections. After heavily binning the spectrum, we estimate the line to be significant at the $\gtrsim 4\sigma$ level. We measure the flux-weighted, systemic CO redshift as $z_{\mathrm{CO}} = 3.099 \pm 0.004$. A Gaussian fit to the spectrum yields a linewidth of FWHM $= 780 \pm 100\,\mathrm{km\,s^{-1}}$ and a line flux density of $I_{\mathrm{CO}} = 0.8 \pm 0.2\,\mathrm{Jy\,km\,s^{-1}}$.

Contours of the velocity-integrated CO emission are shown on a $K$-band image in Fig. 2(e). The CO emission is detected at the $\sim 4.7\sigma$ level ($\sigma = 0.17\,\mathrm{mJy\,beam^{-1}}$), at a position offset by $\sim 2.5$ arcsec north-west from the optical counterpart, but only $\sim 0.8$ arcsec away from the radio position (phase centre).

### 3.6 Non-detections

In Table 2, we list the $3\sigma$ upper limits on the 3-mm CO line flux spatially coincident with the radio position as well as the redshift range searched for each of the six non-detections. The upper limits were calculated using the equation $I_{\mathrm{CO}} = 3\sigma(\delta v \Delta v_{\mathrm{FWHM}})^{1/2}$, where $\sigma$ is the channel-to-channel rms noise, $\delta v$ the velocity resolution and $\Delta v_{\mathrm{FWHM}}$ the linewidth (see e.g. Seaquist, Ivison & Hall 1995). In our calculation of the upper limits, we used the rms noise in the spectra binned to 100 MHz resolution and adopted a linewidth of $500\,\mathrm{km\,s^{-1}}$. The integrated CO(3–2) map of SMM J12360+6210

**Table 2.** Submillimetre galaxies (SMGs) observed in CO to date, including the submm-bright ERO J16450+4626, which although not selected in the submm is thought to be similar to the submillimetre galaxy (SMG) population. The top section of the table lists the five new CO detections presented here and the three previously published detections from our survey (Neri et al. 2003); the six non-detected SMGs are listed in the middle section, while the sources from the literature are given in the bottom section of the table.

| Source name | Transition | CO position | | Optical/NIR position | | Radio position | | $z_{\rm spec}$ | $z_{\rm CO}$ | $\Delta V_{\rm FWHM}$ | $I_{\rm CO}$ | Ref. |
|---|---|---|---|---|---|---|---|---|---|---|---|---|
| | | $\alpha_{\rm J2000}$ (h m s) | $\delta_{\rm J2000}$ (° ′ ″) | $\alpha_{\rm J2000}$ (h m s) | $\delta_{\rm J2000}$ (° ′ ″) | $\alpha_{\rm J2000}$ (h m s) | $\delta_{\rm J2000}$ (° ′ ″) | | | (km s$^{-1}$) | (Jy km s$^{-1}$) | |
| **Detections** | | | | | | | | | | | | |
| SMM J02396−0134[a,b] | (2–1) | 02 39 56.59 | −01 34 26.6 | 02 39 56.51 | −01 34 25.66 | 02 39 56.30 | −01 34 30.8 | $1.062 \pm 0.001$[c] | $1.062 \pm 0.002$ | $780 \pm 60$ | $3.4 \pm 0.3$ | (1) |
| SMM J13120+4242 | (4–3) | 13 12 01.20 | +42 42 08.8 | 13 12 01.23 | +42 42 08.2 | 13 12 01.17 | +42 42 08.1 | $3.405 \pm 0.001$[d] | $3.408 \pm 0.002$ | $530 \pm 50$ | $1.7 \pm 0.3$ | (1) |
| SMM J16366+4105 | (3–2) | 16 36 58.23 | +41 05 23.7 | 16 36 58.21 | +41 05 23.9 | 16 36 58.19 | +41 05 23.8 | $2.454 \pm 0.001$[d] | $2.450 \pm 0.002$ | $870 \pm 80$ | $1.8 \pm 0.3$ | (1) |
| SMM J16371+4053 | (3–2) | 16 37 06.50 | +40 53 13.8 | 16 37 06.54 | +40 53 14.1 | 16 37 06.51 | +40 53 13.8 | $2.374 \pm 0.001$[d] | $2.380 \pm 0.004$ | $830 \pm 130$ | $1.0 \pm 0.2$ | (1) |
| SMM J22174+0015 | (3–2) | 22 17 35.20 | +00 15 37.6 | 22 17 34.95 | +00 15 33.2 | 22 17 35.15 | +00 15 37.2 | $3.098 \pm 0.002$[d] | $3.099 \pm 0.004$ | $780 \pm 100$ | $0.8 \pm 0.2$ | (1) |
| SMM J04431+0210[a,b] | (3–2) | 04 43 07.25 | +02 10 23.3 | 04 43 07.25 | +02 10 24.4 | 04 43 07.25 | +02 10 24.4 | $2.5092 \pm 0.0008$[e] | $2.5094 \pm 0.0002$ | $350 \pm 60$ | $1.4 \pm 0.2$ | (2) |
| | (7–6) | ... | ... | ... | ... | ... | ... | ... | ... | ... | $\leqslant 0.8$ | (2) |
| SMM J09431+4700[a] | (4–3) | 09 43 03.74 | +47 00 15.3 | 09 43 03.70[f] | +47 00 15.1[f] | 09 43 03.7 | +47 00 15.1 | $3.349 \pm 0.001$[d] | $3.3460 \pm 0.0001$ | $420 \pm 50$ | $1.1 \pm 0.1$ | (2) |
| | (9–8) | ... | ... | ... | ... | ... | ... | ... | ... | ... | $\leqslant 1.0$ | (2) |
| SMM J16368+4057 | (3–2) | 16 36 50.43 | +40 57 34.7 | 16 36 50.40 | +40 57 34.2 | 16 36 50.43 | +40 57 34.5 | $2.380 \pm 0.002$[d] | $2.3853 \pm 0.0014$ | $840 \pm 110$ | $2.3 \pm 0.2$ | (2) |
| | (7–6) | 16 36 50.41 | +40 57 34.3 | ... | ... | ... | ... | ... | $2.383 \pm 0.002$ | ... | $1.1 \pm 0.2$ | (2) |
| **Non-detections** | | | | | | | | | | | | |
| SMM J10523+5722 | (3–2) | ... | ... | 10 52 30.75 | +57 22 09.4 | 10 52 30.73 | +57 22 09.5 | $2.611 \pm 0.001$[d] | 2.5901 − 2.6119 | ... | $\leqslant 0.6$[g] | (1) |
| SMM J10524+5724 | (3–2) | ... | ... | 10 52 38.34 | +57 24 36.0 | 10 52 38.30 | +57 24 35.8 | $3.036 \pm 0.001$[d] | 3.0593 − 3.0318 | ... | $\leqslant 1.0$[g] | (1) |
| SMM J12360+6210 | (3–2) | ... | ... | 12 36 00.12 | +62 10 47.7 | 12 36 00.20 | +62 10 47.0 | $1.994 \pm 0.001$[d] | 1.9865 − 2.0015 | ... | $\leqslant 1.3$[g] | (1) |
| SMM J13123+4239 | (3–2) | ... | ... | 13 12 32.31 | +42 39 49.5 | 13 12 32.30 | +42 39 50.0 | $2.320 \pm 0.001$[d] | 2.3115 − 2.3300 | ... | $\leqslant 1.4$[g] | (1) |
| SMM J16363+4055 | (3–2) | ... | ... | 16 36 31.47 | +40 55 46.6 | 16 36 31.47 | +40 55 46.9 | $2.283 \pm 0.001$[d] | 2.2676 − 2.2919 | ... | $\leqslant 0.6$[g] | (1) |
| SMM J16363+4056 | (2–1) | ... | ... | 16 36 39.16 | +40 56 35.9 | 16 36 39.01 | +40 56 35.9 | $1.495 \pm 0.001$[d] | 1.4802 − 1.5001 | ... | $\leqslant 1.4$[g] | (1) |
| **Literature sources** | | | | | | | | | | | | |
| SMM J02399−0136[a,b] | (3–2) | 02 39 51.89 | −01 35 58.9 | 02 39 51.88 | −01 35 58.0 | 02 39 51.88 | −01 35 58.0 | $2.803 \pm 0.003$[d] | $2.808 \pm 0.002$ | $710 \pm 80$ | $3.0 \pm 0.4$ | (3) |
| | (3–2) | 02 39 51.87 | −01 35 58.8 | 02 39 51.85 | −01 35 58.2 | ... | ... | ... | $2.8076 \pm 0.0002$ | $\geqslant 1100$ | $3.1 \pm 0.4$ | (4) |
| SMM J14011+0252[a,b] | (3–2) | 14 01 04.92 | +02 52 25.6 | 14 01 04.95 | +02 52 24.0 | 14 01 04.96 | +02 52 23.5 | $2.562 \pm 0.002$[d] | $2.5653 \pm 0.0003$ | $200 \pm 40$ | $2.4 \pm 0.3$ | (5) |
| | (3–2) | 14 01 04.93 | +02 52 24.1 | ... | ... | ... | ... | ... | $2.5652 \pm 0.0001$ | $190 \pm 11$ | $2.8 \pm 0.3$ | (6) |
| | (7–6) | 14 01 04.92 | +02 52 23.8 | ... | ... | ... | ... | ... | $2.5651 \pm 0.0002$ | $170 \pm 30$ | $3.2 \pm 0.5$ | (6) |
| SMM J16359+6612[a,b] | (3–2) | 16 35 54.15 | +66 12 24 | 16 35 54.19 | +66 12 24.9 | ... | ... | $2.5165 \pm 0.0015$[e] | $2.5168 \pm 0.0003$ | $500 \pm 100$ | $3.5 \pm 0.1$ | (7) |
| | (3–2) | 16 35 54.10 | +66 12 23.8 | ... | ... | ... | ... | ... | $2.5174 \pm 0.0002$ | $500 \pm 100$ | $2.50 \pm 0.12$ | (8) |
| ERO J16450+4626[b] | (2–1) | 16 45 02.26 | +46 26 26.5 | 16 45 02.36 | +46 26 25.5 | ... | ... | $1.443 \pm 0.001$[e] | $1.439 \pm 0.001$ | $400 \pm 20$ | $1.40 \pm 0.10$ | (8) |
| | (5–4) | ... | ... | ... | ... | ... | ... | ... | $1.440 \pm 0.001$ | $380 \pm 20$ | $1.35 \pm 0.10$ | (9) |
| | (1–0) | ... | ... | ... | ... | ... | ... | ... | ... | ... | $0.6 \pm 0.1$ | (10) |

[a]The source is lensed; see Table 3 for magnifications $\mu_{\rm L}$.[b]The CO emission is extended. [c]The redshift is derived from the O II λ3727 line (Soucail et al. 1999). [d] The redshift is derived from Lyα (Ivison et al. 2000; Ledlow et al. 2002; Smail et al. 2003; Chapman et al. 2005). [e] The redshift is derived from Hα (Dey et al. 1999; Frayer et al. 2003; Kneib et al. 2004; Swinbank et al. 2004). [f] Position of H7; see Neri et al. (2003) for details. [g]The 3$\sigma$ upper limits have been calculated over an assumed velocity range of 500 km s$^{-1}$.

References: (1) this work; (2) Neri et al. (2003); (3) Frayer et al. (1998); (4) Genzel et al. (2003); (5) Frayer et al. (1999); (6) Downes & Solomon (2003); (7) Sheth et al. (2004); (8) Kneib et al. (2004); (9) Andreani et al. (2000); (10) Greve et al. (2003).

shows an $\sim 4\sigma$ peak slightly eastwards of the phase centre and is thus possibly another tentative detection, albeit marginal. In the remaining cases, no line emission is observed at a significance $\geqslant 3\sigma$.

## 4 SAMPLE PROPERTIES

### 4.1 The sample

The main goal of this paper is to assemble a large sample of SMGs observed in CO. In order to achieve this, we add to the 11 new sources in Table 1 from our survey (detections as well as non-detections) and the three earlier CO detections from this survey described in Neri et al. (2003), the three SMGs detected in CO prior to our survey: SMM J02399−0136 (Frayer et al. 1998; Genzel et al. 2003), SMM J14011+0252 (Frayer et al. 1999; Downes & Solomon 2003) and SMM J16359+6612 (Kneib et al. 2004; Sheth et al. 2004). The latter is a triply imaged lensed galaxy with CO detected towards all three components and in Fig. 1(h) we have displayed the combined (and therefore highest signal-to-noise ratio) spectrum of all three components as given in Kneib et al. (2004). For the velocity-integrated line flux, we have adopted the value of the component with the strongest detection, i.e. component B (Kneib et al. 2004; see Table 2).

We also include the extremely red object, HR 10, at $z = 1.443$ (ERO J16450+4626; Hu & Ridgway 1994). Initially studied because of its extremely red optical–near-infrared colours, subsequent observations with SCUBA and the *Hubble Space Telescope* (*HST*) revealed that HR 10 is a powerful SMG with a distorted rest-frame UV morphology (e.g. Cimatti et al. 1998; Dey et al. 1999). Hence, HR 10 bears all the characteristics of an SMG and would have been detected in any of the SCUBA surveys to date. The CO(5–4), CO(2–1) and CO(1–0) lines have all been detected towards this source (Andreani et al. 2000; Greve, Ivison & Papadopoulos 2003).

Finally, we note that Hainline et al. (2004) detected CO(3–2) towards the submm source SMM J04135+10277, the first type 1 QSO to be selected at submm wavelengths (Knudsen, van der Werf & Jaffe 2003), as part of an Owens Valley Millimeter Array survey of CO emission towards high-redshift QSOs. SMM J04135+10277 is not only one of the brightest submm sources known but also an extremely luminous CO source. While SMM J04135+10277 was discovered in a blank-field (albeit lensing-assisted) submm survey and thus meets the selection criteria for our sample, only approximately 3 per cent of radio-identified SMGs are broad-line QSOs (Chapman et al. 2005), suggesting that this source is not representative of the SMG population as a whole. SMM J04135+10277 is therefore not included in our sample of CO-detected SMGs.

The final SMG sample consists of 12 CO detections and six non-detections; their observational properties are listed in Table 2. The CO line profiles of the 12 detected sources are shown in Fig. 1. In the following sections, we shall use the CO observations to investigate the physical properties of the SMG population (see Table 3). In the case where an SMG is known to be gravitationally lensed, we have corrected the luminosities, gas masses and linear sizes, etc., using the gravitational lensing magnification factors listed in Table 3.

### 4.2 Comparison of optical and CO redshifts

In general, CO lines provide excellent systemic redshifts for galaxies, by tracing the extended molecular gas distribution rather than the ionized gas produced by shocked outflows or accretion on to an AGN. The latter is typically traced by high ionization, e.g. broad C IV λ1549 lines, which have been shown to be systematically blueshifted with respect to the systemic redshift in quasars (e.g. Richards et al. 2002), and by the Ly$\alpha$ line, which in the majority of high-redshift CO detections is blueshifted with respect to the CO redshift as a result of outflows and dust obscuration (e.g. Hainline et al. 2004). The purpose of this section is to determine if similar systematic offsets between the CO and Ly$\alpha$ redshifts exist within the SMG population. We have measurements of the Ly$\alpha$ redshifts for eight of the CO-detected SMGs (see Table 2).

**Table 3.** Physical properties derived from the CO observations.

| Source | $\mu_{\rm L}$[a] | $D$(1 arcsec)[b] (kpc) | Transition | $L'_{\rm CO}$[b] ($\times 10^{10}$ K km s$^{-1}$ pc$^2$) | $M({\rm H_2})$[b,c] ($\times 10^{10}$ M$_\odot$) | $\Delta V_{\rm FWHM}$[d] (km s$^{-1}$) | $M_{\rm dyn}$[e] ($\times 10^{11}$ M$_\odot$) |
|---|---|---|---|---|---|---|---|
| SMM J02396−0134 | 2.5 | 3.3 | (2–1) | $2.1 \pm 0.2$ | $1.7 \pm 0.2$ | $780 \pm 60$ | 1.2 |
| SMM J02399−0136 | 2.5 | 3.2 | (3–2) | $4.8 \pm 0.8$ | $3.8 \pm 0.6$ | $1360 \pm 50$ | 3.5 |
| SMM J04431+0210 | 4.4 | 1.9 | (3–2) | $1.1 \pm 0.2$ | $0.9 \pm 0.2$ | $350 \pm 60$ | 0.1 |
| SMM J09431+4700 | 1.2 | 6.3 | (4–3) | $2.7 \pm 0.3$ | $2.2 \pm 0.2$ | $420 \pm 50$ | 0.7 |
| SMM J10523+5722 | 1.0 | 8.1 | (3–2) | $\leqslant 2.1$ | $\leqslant 1.4$ | ... | ... |
| SMM J10524+5724 | 1.0 | 7.8 | (3–2) | $\leqslant 4.6$ | $\leqslant 3.0$ | ... | ... |
| SMM J12360+6210 | 1.0 | 8.5 | (3–2) | $\leqslant 2.9$ | $\leqslant 1.6$ | ... | ... |
| SMM J13120+4242 | 1.0 | 7.5 | (4–3) | $5.3 \pm 0.9$ | $4.2 \pm 0.7$ | $530 \pm 50$ | 1.2 |
| SMM J13123+4239 | 1.0 | 8.3 | (3–2) | $\leqslant 4.1$ | $\leqslant 2.4$ | ... | ... |
| SMM J14011+0252[f] | 5.0 | 1.6 | (3–2) | $1.9 \pm 0.2$ | $1.5 \pm 0.2$ | $190 \pm 11$ | 0.03 |
| SMM J16368+4057 | 1.0 | 8.3 | (3–2) | $7.0 \pm 0.6$ | $5.6 \pm 0.5$ | $840 \pm 110$ | 3.5 |
| SMM J16359+6612 | 22 | 0.4 | (3–2) | $0.4 \pm 0.2$ | $0.3 \pm 0.2$ | $500 \pm 100$ | 0.06 |
| SMM J16363+4055 | 1.0 | 8.3 | (3–2) | $\leqslant 1.7$ | $\leqslant 0.9$ | ... | ... |
| SMM J16363+4056 | 1.0 | 8.5 | (2–1) | $\leqslant 4.1$ | $\leqslant 1.8$ | ... | ... |
| SMM J16366+4105 | 1.0 | 8.2 | (3–2) | $5.7 \pm 1.0$ | $4.6 \pm 0.7$ | $870 \pm 80$ | 3.7 |
| SMM J16371+4053 | 1.0 | 8.3 | (3–2) | $3.0 \pm 0.9$ | $2.4 \pm 0.7$ | $830 \pm 130$ | 3.4 |
| ERO J16450+4626 | 1.0 | 8.5 | (2–1) | $3.8 \pm 0.3$ | $3.0 \pm 0.2$ | $400 \pm 20$ | 0.8 |
| SMM J22174+0015 | 1.0 | 7.8 | (3–2) | $3.8 \pm 1.0$ | $3.0 \pm 0.7$ | $780 \pm 100$ | 2.8 |
| Median[g] | | $7.5 \pm 3.1$ | | $3.8 \pm 2.0$ | $3.0 \pm 1.6$ | $780 \pm 320$ | $1.2 \pm 1.5$ |

[a]Assuming equal flux magnification and linear magnification. [b]$D$(1 arcsec) is the linear distance in kpc corresponding to 1 arcsec at the given redshift and corrected for the lensing amplification $\mu_{\rm L}$. [c]Derived assuming $X_{\rm CO} = 0.8$(K km s$^{-1}$ pc$^2$)$^{-1}$ M$_\odot$. [d]The linewidths are derived from a single Gaussian fit to the line profile. [e]Calculated adopting a source diameter of 0.5 arcsec. [f]The amplification factor for this source was recently revised from 2.5 to $\sim 5$ (see discussion in Swinbank et al. 2004). [g]The non-detections (upper limits) are not included in the median.

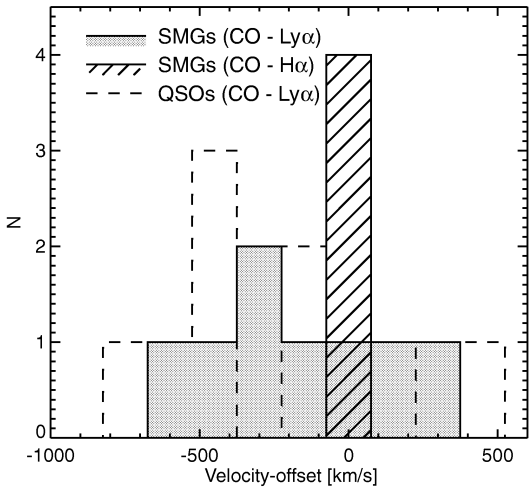


**Figure 3.** The histograms show the distribution of velocity differences derived from the redshifts from CO line observations and rest-frame UV spectroscopy. We show the distribution for the eight submillimetre galaxies (SMGs) for which spectroscopic redshifts have been derived from the Ly$\alpha$ line (grey shaded histogram) and for the 15 quasi-sellar objects (QSOs) in Table 4 (two of the QSOs have velocity offsets $\lesssim -1000\,\mathrm{km\,s^{-1}}$). The hashed histogram compares the redshifts between the CO and H$\alpha$ emission line for the four SMGs with redshifts derived from H$\alpha$ (three) or [O II] $\lambda$3727 Å (one). The bin size is $150\,\mathrm{km\,s^{-1}}$, which also reflects the typical error in the velocity offsets.

A large fraction of CO line profiles shown in Fig. 1 are double peaked or asymmetric, making it difficult to accurately determine the CO redshift by fitting Gaussian profiles to the spectra. Instead, the CO redshift of a source was determined by computing its flux-weighted redshift, i.e. $z_{\rm CO} = \sum I(z)z / \sum I(z)$. The error on the redshift is given by $\Delta z^2_{\rm CO} = \sum I(z)(z - z_{\rm CO})^2 / \sum I(z)$. The CO redshifts computed in this way are listed in Table 2.

In Fig. 3, we have plotted the distribution of velocity offsets corresponding to the differences between the CO and Ly$\alpha$ redshifts for the SMG sample. Negative velocity offsets correspond to blueshifted UV emission with respect to the systemic CO redshift. Also shown are the velocity offsets for the four SMGs with H$\alpha$ redshifts.

The velocity offsets between the Ly$\alpha$ and CO redshifts of SMGs show a tendency for blueshifted offsets (five and two SMGs have blueshifted and redshifted offsets, respectively, with one source consistent with no velocity offset within the errors, $\sim 150\,\mathrm{km\,s^{-1}}$), although this needs to be confirmed once a larger sample of SMGs is studied. The 15 QSOs detected in CO to date show a similar tentative excess of negative CO–Ly$\alpha$ velocity offsets (Fig. 3), although in this case the the shift is a result of the strong absorption of the line: most likely from gas on small scales near the nucleus. In the case of SMGs, the offsets are likely to come from absorption from a wind on larger kpc scales: where we only see the line scattered from the far side of the wind/shell as a result of the absorption of the blueshifted component.

It is clear from Fig. 3 that, in the majority of the SMGs, significant velocity offsets exist between the Ly$\alpha$ and CO emission. Such large offsets illustrate how easy it would be to miss a CO line based on blind tuning to the rest-frame UV redshift and highlight the need for future submm/mm correlators with large instantaneous bandwidths.

Realizing the potential danger of not detecting some of the SMGs because of large offsets between the CO and rest-frame UV redshifts, we have undertaken a programme to target SMGs using the near-infrared spectrographs (NIRSPEC) on Keck-II, the OH-Airglow Suppressor (OHS) on Subaru and the Infrared Spectrometer And Array Camera (ISAAC) on the Very Large Telescope (VLT) to allow us to measure redshifts from rest-frame optical emission lines, which should provide more reliable estimates of the systemic redshifts (e.g. Simpson et al. 2004; Swinbank et al. 2004). The usefulness of this approach is demonstrated by the hashed histogram in Fig. 3, which shows that for the four SMGs with redshifts derived from H$\alpha$ (or [O II] $\lambda$3727 Å in the case of SMM J02396−0134, Soucail et al. 1999), the velocity offsets amount to no more than $\pm\,75\,\mathrm{km\,s^{-1}}$.

### 4.3 CO luminosities and gas masses

The CO line luminosities, $L'_{\rm CO}$, of the individual SMGs were derived from their velocity-integrated line flux densities following Solomon et al. (1997; SO97) and corrected for gravitational lensing if necessary (see Table 3). For the eight sources detected in CO(3–2), we find a median luminosity of $\langle L'_{\rm CO(3-2)}\rangle = (3.8 \pm 2.3) \times 10^{10}\,\mathrm{K\,km\,s^{-1}\,pc^2}$. Two sources were detected in CO(4–3) (SMM J09431+4700 and SMM J13120+4242) and two in CO(2–1) (SMM J02399−0134 and ERO J16450+4626). Note that for HR 10/ERO J16450+4626 we have used the CO(2–1) spectrum (Andreani et al. 2000) rather than the CO(1–0) measurement by Greve et al. (2003), which lacks velocity information.

Assuming intrinsic velocity/area-averaged brightness temperature line ratios corresponding to an optically thick, thermalized gas, i.e. $r_{32} = T_{\rm b}(3-2)/T_{\rm b}(1-0) = L'(3-2)/L'(1-0) = 1$, and similarly $r_{43} = 1$ and $r_{21} = 1$, we derive a median CO(1–0) luminosity of $\langle L'_{\rm CO(1-0)}\rangle = (3.8 \pm 2.0) \times 10^{10}\,\mathrm{K\,km\,s^{-1}\,pc^2}$, where we have included all sources, except for the non-detections. If we assume more realistic values of $r_{32} = 0.64$ (Devereux et al. 1994), $r_{43} = 0.45$ (Papadopoulos et al. 2000) and $r_{21} = 0.9$ (e.g. Braine & Combes 1992; Aalto et al. 1995) as derived from interstellar medium (ISM) studies in local starburst galaxies, we instead find a median CO(1–0) luminosity of $\langle L'_{\rm CO(1-0)}\rangle = (5.9 \pm 3.6) \times 10^{10}\,\mathrm{K\,km\,s^{-1}\,pc^2}$.

The observed CO luminosities are converted into molecular gas masses using $M(\mathrm{H_2}) = X_{\rm CO} L'_{\rm CO(1-0)}$, where $X_{\rm CO} = 0.8(\mathrm{K\,km\,s^{-1}\,pc^2})^{-1}\,\mathrm{M_\odot}$ is the conversion factor appropriate for UV-intense environments, as derived from observations of local ULIRGs (Downes & Solomon 1998). The molecular gas masses derived for each source are given in Table 3 for assumed (2–1)/(1–0), (3–2)/(1–0) and (4–3)/(1–0) line ratios of unity. The distribution of SMG molecular gas masses is shown in Fig. 4, from which we derive a median value $\langle M(\mathrm{H_2})\rangle = (3.0 \pm 1.6) \times 10^{10}\,\mathrm{M_\odot}$ (not including the upper limits from the non-detections). Given the modest size of our sample, we are not in a position to disentangle the observed scatter in the distribution of molecular gas masses into the separate components caused by varying inclination angles, differences in excitation conditions and underlying scatter in the mass distribution of SMGs.

Because these molecular gas mass estimates are based on observations of high-$J$ CO transitions with $J \geqslant 2$ and made assuming a thermalized, optically thick gas, it is possible that significant amounts of cold, possibly subthermal, molecular gas could be present, but only detectable in lower CO transitions (e.g. Papadopoulos et al. 2001; Papadopoulos & Ivison 2002; Greve et al. 2003). Furthermore, if metal-poor gas is present, the gas mass could be higher. Finally, CO is primarily a tracer of material in the diffuse ISM, and it is possible that a significant amount of dense and clumpy gas ($\gtrsim 10^4\,\mathrm{cm^{-3}}$) is missed by our observations (e.g. Carilli et al. 2005). The quoted $\mathrm{H_2}$ masses in Table 3 should therefore be considered as lower limits to the total amount of molecular gas.

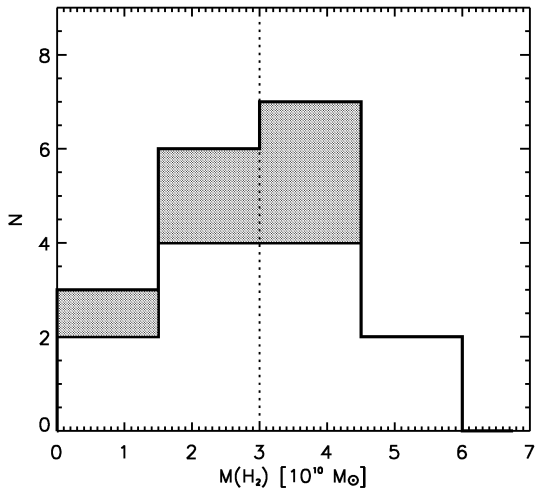


**Figure 4.** The distributions of molecular gas masses of the submillimetre galaxy (SMG) sample assuming a conversion factor of $X_{\rm CO} = 0.8({\rm K\,km\,s^{-1}\,pc^2})^{-1}\,{\rm M_\odot}$ and line ratios $r_{32} = r_{43} = 1$. Non-detections are included as the shaded part of the histogram. The median gas mass of the sample, not including the non-detections, is $\langle M({\rm H_2})\rangle = (3.0 \pm 1.6) \times 10^{10}\,{\rm M_\odot}$ (dotted vertical line).

Our estimates of the molecular gas mass include a non-negligible fraction of Helium, which is accounted for in the adopted value of the conversion factor (Downes & Solomon 1998). The amount of neutral gas (H I), however, is particular difficult to determine and significant uncertainty is associated with $M$(HI) estimates at high redshift (e.g. De Breuck et al. 2003a). Estimates of the $H_2$-to-HI mass ratio in infrared-luminous *IRAS* galaxies range from $\sim 0.5$ in systems with $L_{\rm FIR} \sim 10^{10-11}\,{\rm L_\odot}$ (Andreani, Casoli & Gerin 1995) to $\sim 4$ for $L_{\rm FIR} \sim 10^{12}\,{\rm L_\odot}$ systems (Mirabel & Sanders 1989). The latter value may apply to the extremely far-infrared luminous SMGs. However, most of the neutral gas in local galaxies is on very large scales ($\gtrsim 10$ kpc) and thus may not be relevant for our estimates.

Finally, we have looked for evidence of a correlation between molecular gas content and redshift. Such a trend would be indicative of evolution within the redshift range spanned by the SMG population. If we only consider the 13 sources observed in CO as part of our statistically complete survey (i.e. not including SMM J02396−0134) and split the sample into low- and high-redshift halves at the median redshift of the sample, $\langle z\rangle = 2.4$, we find that the CO detection rate in the high-redshift ($z \geqslant 2.4$) subset is 5/7 (71 per cent) compared with just 2/6 (33 per cent) for sources at $z < 2.4$. The higher detection rate at $z \geqslant 2.4$ could be indicative of evolution over the redshift range $z \sim 1$–3 in the gas masses associated with the most luminous starbursts. Using a Cox/Hazard survival analysis, we find that the formal likelihood of a variation in detection rate with redshift in the 13 sources observed by our survey is $P = 0.995$, suggestive of a real trend. If we instead include all the sources listed in Table 2, the trend weakens (the detection rates become 4/8 and 8/10 for the low- and high-redshift bins, respectively). This is unsurprising because the bias against publishing non-detections in the literature means that this comparison is less reliable than that for our statistically complete sample.

### 4.4 Linewidths and dynamical masses

A striking feature of the SMG population is their typically broad CO line profiles (Table 3). The median observed FWHM of the sample is $780 \pm 320\,{\rm km\,s^{-1}}$ and the median FWZI is $850\,{\rm km\,s^{-1}}$. These values do not take into account any geometrical effects, such as inclination angle, which could effect the individual estimated linewidths by more than a factor of 2. For example, in the case of SMM J14011+0252 it is plausible that the relatively small linewidth is a result of the fact that the angular momentum vector of the system is closely aligned to our line of sight (Tecza et al. 2004). Hence, the observed FWHM are firm lower limits to the true orbital velocities and, assuming our sample has random orbital inclinations, then the average correction should be a factor of sec $\pi/4 = 1.4$.

In order to use our observed CO linewidths to derive the dynamical mass of the SMGs, we must know the spatial extent of the CO. However, so far CO emission has been reliably resolved in only one SMG: SMM J02399−0136 (Genzel et al. 2003). While a number of SMGs show tentative evidence of extended CO emission (Ivison et al. 2001; Greve et al. 2003; Neri et al. 2003), their low signal-to-noise ratios prevent a robust determinations of the source size. Instead, we have assumed a conservative source diameter of $\sim 0.5$ arcsec, which corresponds to a median linear diameter of 3.7 kpc (correcting for gravitational lensing where relevant; see Table 3). This is a factor of 2 smaller than the source sizes estimated by Neri et al. (2003), but consistent with characteristic size estimates from recent high-resolution radio observations of SMGs with the multi-element radio-linked interferometer network (MERLIN) by Chapman et al. (2004) and with results from high-resolution PdBI CO observations (Tacconi et al. 2005) of the three SMGs detected in CO by Neri et al. (2003).

Another notable feature of our sample is the high fraction of SMGs that show evidence of double-peaked CO line profiles. Four sources (SMM J02396−0134, SMM J02399−0136, SMM J16359+6612 and SMM J16366+4105) show unambiguous double-peaked profiles and a further two sources (SMM J04431+0210 and SMM J16368+4057) are better fit by a double Gaussian than a single Gaussian, as measured by the reduced $\chi^2$ of the fit. In the case of SMM J16368+4057, further evidence of multiple CO peaks comes from H$\alpha$ UKIRT/UIST integral field unit (IFU) observations (Swinbank et al. 2005), which show emission components at velocity offsets similar to those we infer from the double Gaussian fit. Thus, at least 4/12 (33 per cent) and possibly as many as 6/12 (50 per cent) of the detected sample show evidence of having more than one CO-emitting component in their spectra. Comparing the occurrence of double-peaked line profiles in sources as a function of redshift within our sample, we see that the double-peaked sources appear to lie at the lower-redshift end of our sample, 5/7 at $z \leqslant 2.5$, compared with 1/5 for the SMGs at $z > 2.5$. A possible explanation for this tentative trend is discussed later.

Such multipeaked line profiles are a telltale sign of orbital motion under the influence of gravity and can usually be attributed to either a disc or a merger. To determine the likely structure of the gas reservoir, we use our median gas mass ($3 \times 10^{10}\,{\rm M_\odot}$) and adopt a typical diameter of $\sim 4$ kpc for the gas reservoir, to derive a mass surface density of ($\Sigma \sim 2.4 \times 10^3\,{\rm M_\odot\,pc^{-2}}$) for this structure. This is extremely high and implies that if the gas is present in a disc then this will have a Toomre parameter $Q < 1$,[2] indicating it will be unstable to bar formation. The disc would then collapse on a timescale comparable to the sound crossing time, which is much shorter

[2] Toomre's stability criterion says that $Q = \frac{2v_{\rm s}\Omega}{\pi G\Sigma} \geqslant 1$ in order for a gaseous disc to be stable: see e.g. Binney & Tremain (1987). For a surface density $\Sigma \sim 2.4 \times 10^3\,{\rm M_\odot\,pc^{-2}}$, $Q$ will always be less than 1 for any realistic values of the sound speed $v_{\rm s}$ and circular frequency $\Omega$.

than the expected $\sim$10–100 Myr duration of the SMG phase (see Section 5.4). We conclude that the kinematics responsible for the double-peaked CO lines are unlikely to arise from gas distributed in a stable disc, instead a more likely scenario is that they reflect a merger of two gas-rich components or from a disc collapsing under gravitational instability.

With almost all of the SMGs being spatially unresolved in CO, we are unable to determine whether SMGs typically contain gaseous discs in their centres or if they are mergers. However, given their large gas mass densities, as well as the high fraction of double-peaked profiles, we feel that SMGs are more likely to be mergers. Additional evidence for a merger origin comes from the detection of close companions in CO in some of our fields (Neri et al. 2003), as these these are likely to be interacting or merging given the small spatial and velocity differences. Thus, dynamical masses were calculated using the merger formula given in Neri et al. (2003; see also Genzel et al. 2003) and reported in Table 3. Neri et al. (2003) assumed a stable disc model that gives dynamical masses lower by a factor of 2; but because they adopted a characteristic source size twice as large as ours, the resulting dynamical mass estimates coincide. The median SMG dynamical mass within $R \lesssim 2$ kpc is $\langle M_{\rm dyn}\rangle \simeq (1.2 \pm 1.5) \times 10^{11}\,{\rm M}_{\odot}$, where we have applied an average correction of a factor of 1.4, assuming random inclinations for the sample overall. We estimate a median molecular gas to dynamical mass fraction in SMGs of $\langle M_{\rm gas}/M_{\rm dyn}\rangle \sim 0.3$ ($\sim$0.5 if we assume a disc model). This indicates that the contribution of the gas reservoir to the dynamics of the central regions of typical SMGs is substantial and that the gas has already concentrated into the central regions of the galaxy by some dissipative process. It should be noted, however, that significant uncertainties are associated with the dynamical mass estimates, especially if the system is not in dynamical equilibrium, or if the observed line is not a good tracer of the dynamical state of the galaxy (also see the discussion in Neri et al. 2003).

## 5 COMPARISON WITH OTHER POPULATIONS

Unlike optical/near-infrared and X-ray observations, CO observations are relatively unaffected by either dust extinction or AGN activity, and a comparison between the CO properties of SMGs and that of other galaxy populations could therefore potentially provide us with a clean way of comparing the bulk properties of SMGs with other galaxy populations at both high and low redshifts; although, by virtue of the submm selection technique, such a comparison is of course biased towards dust-enshrouded sources.

We list in Table 4 all non-SMG CO sources detected at $z \geqslant 1$. The bulk of these are extreme AGN such as submm-bright, HzRGs or QSOs (e.g. Omont et al. 1996; Papadopoulos et al. 2000; Cox et al. 2002).

As a result of their similar properties, in particular their large far-infrared luminosities, distorted morphologies and optical/near-infrared colours (e.g. Ivison et al. 2002; Smail et al. 2004), SMGs are commonly thought to be high-redshift analogues of local ULIRGs. To test this claim, we now compare the CO properties of SMGs with ULIRGs. To this end, we have used the samples of Sanders, Scovillle & Soifer (1991; SA91) and SO97, which consist of 48 and 37 local ULIRGs [and some luminous infrared galaxies (LIRGs) that are slightly less luminous than the ULIRGs] in the redshift range $z = 0.03$–$0.27$, respectively, and the sample of 60 (U)LIRGs from Yao et al. (2003; Y03), selected from the SCUBA Local Universe Galaxy Survey (SLUGS; Dunne et al. 2000).

### 5.1 CO luminosities and gas masses

In Fig. 5, we plot the CO luminosities of the SMG sample as a function of redshift along with the CO(1–0) luminosities of the (ultraluminous) luminous infrared galaxy (LIRG) samples of SA91, SO97 and Y03. From Fig. 5, it is clear that while the most luminous ULIRGs have CO luminosities comparable to those of the faintest detected SMGs, SMGs are generally more CO luminous than the local (U)LIRGs. In Section 4.3, we found the median CO line luminosity of the SMG sample to be $\langle L'_{\rm CO}\rangle = (3.8 \pm 2.0) \times 10^{10}\,{\rm K\,km\,s^{-1}\,pc^2}$, which is almost a factor of 4 greater than the average CO luminosity of the ULIRGs from SO97. Furthermore, while the CO luminosities of the (U)LIRGs are all based on the lowest and least excitation-biased CO(1–0) rotational line, all of the SMGs are detected in higher transitions. Hence, the CO luminosities based on the high-$J$ lines for SMGs should be regarded as lower limits on the CO(1–0) luminosities, unless the lines are fully thermalized at high temperatures and optically thick.

The (U)LIRGs lie on a well-defined locus in Fig. 5, which is extended to the highest redshifts and CO luminosities by the SMG sample. The lower boundary of this trend is determined by the sensitivity limits of the CO observations, while the upper bound is a real astrophysical limit. The steady decline in the CO luminosity of SMGs to ULIRGs and LIRGs seen in Fig. 5 is likely to reflect the evolution in the molecular gas content of the most luminous starburst galaxies as a function of redshift, despite the expected increasing mass of a typical galaxy with cosmic time. A possible caveat is the assumption of a constant conversion factor in (U)LIRGs and SMGs. In (U)LIRGs, the $X_{\rm CO}$ conversion factor is approximately 4.5 times lower than in normal spiral galaxies and it is possible that for the yet more luminous SMGs it is even lower.

Also shown in Fig. 5 are the CO luminosities of all HzRGs and QSOs detected to date (Table 4), as well as the only optically selected Lyman break galaxy (LBG), MS 1512−cB58 ($z = 2.73$), detected in CO (Baker et al. 2004). Their large apparent scatter is a result of many of these objects being gravitationally lensed, increasing the effective sensitivity limits of their observations beyond the capabilities of current instruments in blank fields. SMGs are seen to have CO luminosities comparable to the most luminous HzRGs (e.g. Papadopoulos et al. 2000; De Breuck et al. 2003a; De Breuck, Neri & Omont 2003b) and QSOs (e.g. Carilli et al. 2002a; Walter et al. 2003). In contrast, the CO luminosity of the typical-luminosity LBG cB58, $4.2 \times 10^9\,{\rm K\,km\,s^{-1}\,pc^2}$, is nearly 2 orders of magnitude (a factor of $\sim$90) less than the median value for SMGs, despite its similar redshift. With only one LBG detected in CO so far it is not possible to make any meaningful conclusions about the molecular gas content of this population, except that the low CO luminosity of cB58 compared with that of SMGs is consistent with the faintness of Lyman break galaxies (LBGs) at submm wavelengths and their relatively low (compared with SMGs) star formation rates as inferred from optical spectroscopy (Blain et al. 1999; Adelberger & Steidel 2000).

### 5.2 CO linewidths and dynamical masses

In Section 4.4, we found that $\gtrsim$33 per cent of the CO-detected SMGs have double-peaked CO profiles. This is comparable to the fraction of double-peaked CO spectra in local ULIRGs (SO97). The median FWHM CO linewidth for the SMG sample is $780 \pm 320\,{\rm km\,s^{-1}}$, approximately 3 and 4 times larger than the averages for the SA91 and SO97 ultraluminous infrared galaxy (ULIRG) samples, respectively. Because the dynamical mass depends on the square of the

**Table 4.** List of published high-redshift CO detections of Lyman break galaxies (LBGs), quasi-sellar objects (QSOs) and high-redshift radio galaxies (HzRGs). The sources are sorted according to their redshifts. This table, together with Table 2 summarizes the complete list of CO detections of sources at $z \geqslant 1$ to date. The velocity-integrated line fluxes, $I_{\rm CO}$, have not been corrected for gravitational amplification.

| Source | Type | Transition | $z_{\rm spec}$ | $z_{\rm CO}$ | $\Delta V_{\rm FWHM}$ (km s$^{-1}$) | $I_{\rm CO}$ (Jy km s$^{-1}$) | Ref. |
|---|---|---|---|---|---|---|---|
| MS 1512−cB 58[a] | LBG | (3–2) | 2.727 | 2.7265 ± 0.0004 | 174 ± 43 | 0.37 ± 0.08 | (1) |
| Q 0957+561[a] | QSO | (2–1) | 1.413 | 1.414 | 440 | 1.2 | (2),(3) |
| IRAS F10214+4724[a] | QSO | (3–2) | 2.286 | 2.2867 ± 0.0003 | 250 | 21 | (4),(5) |
| | | (3–2) | ... | 2.2855 ± 0.0003 | 230 ± 30 | 4.1 ± 0.9 | (6) |
| | | (3–2) | ... | 2.2854 ± 0.0001 | 220 ± 30 | 4.2 ± 0.8 | (7) |
| | | (6–5) | ... | 2.2857 ± 0.0003 | 240 ± 30 | 9.4 ± 2.0 | (6) |
| H 1413+117[a] | QSO | (3–2) | 2.5582 ± 0.0003 | 2.558 | 326 | 8.1 | (8) |
| | | (3–2) | ... | ... | 352 ± 81 | 14.4 ± 4.4 | (9) |
| | | (3–2) | ... | 2.5579 | 362 ± 23 | 9.9 ± 0.6 | (10) |
| | | (3–2) | ... | 2.55784 ± 0.00003 | 416 ± 6 | 13.2 ± 0.2 | (11) |
| | | (4–3) | ... | 2.5579 | 375 ± 16 | 21.1 ± 0.8 | (10) |
| | | (5–4) | ... | 2.5579 | 398 ± 25 | 24.0 ± 1.4 | (10) |
| | | (7–6) | ... | 2.5579 | 376 | 47.3 ± 2.2 | (10) |
| VCV J1409+5628 | QSO | (3–2) | 2.562 | 2.585 ± 0.001 | 370 ± 60 | 2.4 ± 0.7 | (12) |
| | | (3–2) | ... | 2.5832 ± 0.0001 | 311 ± 28 | 2.3 ± 0.2 | (13) |
| | | (7–6) | ... | ... | ... | 4.1 ± 1.0 | (13) |
| MG 0414+0534[a] | QSO | (3–2) | 2.639 ± 0.002 | 2.639 | 580 | 2.6 | (14) |
| LBQS 1230+1627B | QSO | (3–2) | 2.735 ± 0.005 | 2.741 ± 0.002 | ... | 0.80 ± 0.26 | (15) |
| RX J0911+0551[a] | QSO | (3–2) | 2.800 | 2.796 ± 0.001 | 350 ± 60 | 2.9 ± 1.1 | (12) |
| SMM J04135+1027[a] | QSO | (3–2) | 2.837 ± 0.003 | 2.846 ± 0.002 | 340 ± 120 | 5.4 ± 1.3 | (12) |
| MG 0751+2716[a] | QSO | (4–3) | 3.200 ± 0.001 | 3.200 | 390 ± 38 | 5.96 ± 0.45 | (16) |
| APM 08279+5255[a,b] | QSO | (1–0) | 3.87 | 3.9 | ... | 0.150 ± 0.045 | (17) |
| | | (1–0) | ... | ... | ... | 0.22 ± 0.05 | (18) |
| | | (2–1) | ... | ... | ... | 1.15 ± 0.54 | (17) |
| | | (4–3) | ... | 3.9114 ± 0.0003 | 480 ± 35 | 3.7 ± 0.5 | (19) |
| | | (9–8) | ... | 3.9109 ± 0.0002 | ... | 9.1 ± 0.8 | (19) |
| PSS J2322+1944[a] | QSO | (1–0) | 4.1108 ± 0.0005 | 4.1192 ± 0.0004 | 200 ± 70 | 0.19 ± 0.08 | (20) |
| | | (2–1) | ... | ... | ... | 0.92 ± 0.03 | (20) |
| | | (4–3) | ... | 4.1199 ± 0.0008 | 375 ± 41 | 4.21 ± 0.40 | (21) |
| | | (5–4) | ... | 4.1199 ± 0.0008 | 273 ± 50 | 3.74 ± 0.56 | (21) |
| BRI 1335−0417[b] | QSO | (2–1) | 4.398 ± 0.028 | 4.4074 ± 0.0015 | 420 ± 60 | 0.44 ± 0.08 | (22) |
| | | (5–4) | ... | ... | ... | 2.8 ± 0.3 | (23) |
| BRI 0952−0115[a] | QSO | (5–4) | 4.426 ± 0.020 | 4.4337 ± 0.0006 | 230 ± 30 | 0.91 ± 0.11 | (15) |
| BRI 1202−0725[b] | QSO | (2–1) | 4.69 | ... | ... | 0.49 ± 0.09 | (22) |
| | | (4–3) | ... | ... | 280 ± 30 | 1.5 ± 0.3 | (24) |
| | | (5–4) | ... | 4.6932 ± 0.002 | 320 ± 35 | 2.40 ± 0.30 | (25) |
| | | (5–4) | ... | | 220 ± 74 | 2.7 ± 0.41 | (25) |
| | | (7–6) | ... | 4.6915 ± 0.001 | 250 − 300 | 3.1 ± 0.86 | (24) |
| SDSS J1148+5251 | QSO | (3–2) | 6.43 ± 0.05 | 6.418 ± 0.004 | 320 | 0.18 ± 0.04 | (26) |
| | | (6–5) | ... | 6.4187 ± 0.0006 | 279 | 0.73 ± 0.076 | (27) |
| | | (7–6) | ... | 6.4192 ± 0.0009 | 279 | 0.64 ± 0.088 | (27) |
| 53 W002 | HzRG | (3–2) | 2.390 ± 0.004 | 2.394 ± 0.001 | 540 ± 100 | 1.5 ± 0.2 | (28) |
| | | (3–2) | ... | 2.3927 ± 0.0003 | 420 ± 40 | 1.20 ± 0.15 | (29) |
| B3 J2330+3927[b] | HzRG | (4–3) | 3.087 ± 0.004 | 3.094 | 500 | 1.3 ± 0.3 | (30) |
| TN J0121+1320 | HzRG | (4–3) | 3.516 | 3.520 | 700 | 1.2 ± 0.4 | (31) |
| 6C 1909+722 | HzRG | (4–3) | 3.5356 | 3.532 | 530 ± 70 | 1.62 ± 0.30 | (32) |
| 4C 41.17[b] | HzRG | (4–3) | 3.79786 ± 0.0024 | 3.7958 ± 0.0008 | 1000 ± 150 | 1.8 ± 0.2 | (33) |
| 4C 60.07[b] | HzRG | (1–0) | 3.788 | 3.791 | $\geqslant$ 1000 | 0.24 ± 0.03 | (34) |
| | | (4–3) | ... | 3.791 | ... | 2.50 ± 0.43 | (32) |
| TN J0924−2201 | HzRG | (1–0) | 5.1989 ± 0.0006 | 5.202 ± 0.001 | 250 − 400 | 0.087 ± 0.017 | (35) |
| | | (5–4) | ... | ... | 200 − 300 | 1.19 ± 0.27 | (35) |

[a]The source is gravitationally lensed. [b]The CO emission is resolved.

References: (1) Baker et al. (2004); (2) Planesas et al. (1999); (3) Krips et al. (2004); (4) Brown & Vanden Bout (1991); (5) Solomon et al. (1992a); (6) Solomon, Downes & Radford (1992b); (7) Downes, Solomon & Radford (1995); (8) Barvainis et al. (1994); (9) Wilner, Zhao & Ho (1995); (10) Barvainis et al. (1997); (11) Weiss et al. (2003); (12) Hainline et al. (2004); (13) Beelen et al. (2004); (14) Barvainis et al. (1998); (15) Guilloteau et al. (1999); (16) Barvainis, Alloin & Bremer (2002); (17) Papadopoulos et al. (2001); (18) Lewis et al. (2002); (19) Downes et al. (1999); (20) Carilli et al. (2002b); (21) Cox et al. (2002); (22) Carilli et al. (2002a); (23) Guilloteau et al. (1997); (24) Omont et al. (1996); (25) Ohta et al. (1996); (26) Walter et al. (2003); (27) Bertoldi et al. (2003); (28) Scoville et al. (1997); (29) Alloin, Barvainis & Guilloteau (2000); (30) De Breuck et al. (2003a); (31) De Breuck et al. (2003b); (32) Papadopoulos et al. (2000); (33) De Breuck et al. (2005); (34) Greve, Ivison & Papadopoulos (2004a); (35) Klamer et al. (2005).

velocity dispersion ($M_{\rm dyn} \sim R\sigma^2$), this would naively suggest that the dynamical masses of the SMGs are ∼9–16 times larger than that of ULIRGs (if the gas kinematics sample similar radii in the galaxies). From detailed interferometric studies of the circumnuclear gas in local ULIRGs, Downes & Solomon (1998) find a median dynamical mass of $\sim 6 \times 10^9$ M$_\odot$ within $R \lesssim 0.6$ kpc: approximately 20 times smaller than the mass enclosed within $R \lesssim 2$ kpc in SMGs (see Table 3). Assuming an isothermal mass distribution, the SMGs will have dynamical masses within 0.6 kpc roughly 6 times that of local ULIRGs.

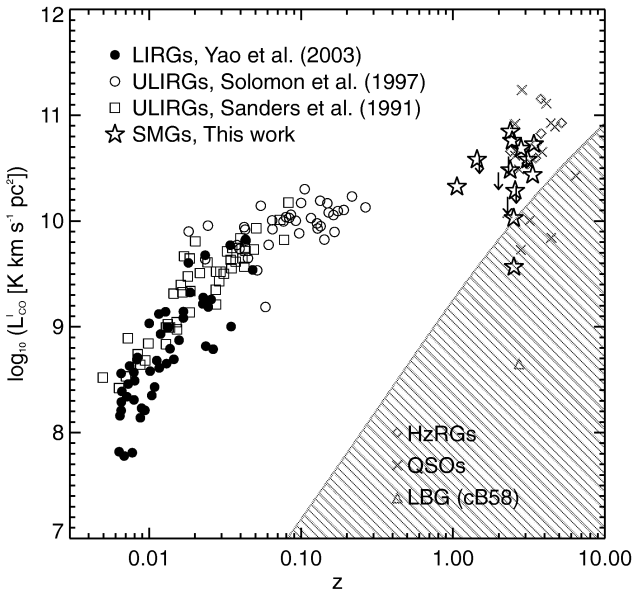


**Figure 5.** The relationship of $\log_{10}(L'_{\rm CO})$ with redshift for the (ultraluminous) luminous infrared galaxy (LIRG) samples of Sanders et al. (1991; SA91), Solomon et al. (1997; SO97) and Yao et al. (2003; Y03), and for the sample of high-redshift (sub)mm-selected sources presented in this paper. The CO luminosities have been corrected for gravitational amplification where necessary. Also shown are the (lensing-corrected) CO luminosities for high-redshift radio galaxies (HzRGs), quasi-sellar objects (QSOs) and Lyman break galaxies (LBGs) listed in Table 4, with the exception of Q 0957+561 and MG 0414+0534, which have unknown gravitational magnification factors. The CO luminosities for the (U)LIRGs are all based on the CO(1–0) line, whereas the luminosities of the high-redshift sources are entirely derived from CO $J = J + 1 \rightarrow J$ transitions with $J + 1 \geqslant 2$ (Table 4). Upper limits on the CO luminosities for the seven SMGs not detected in CO are represented by downward pointing arrows. The hashed area denotes the region where sources are precluded from detection as a result of an integrated CO(3–2) flux limit of $I_{\rm CO} = 0.3\,{\rm Jy\,km\,s^{-1}}$. Of our sample, only SMM J16359+6612 with its very large amplification factor ($\mu = 22$) is detectable below this limit.

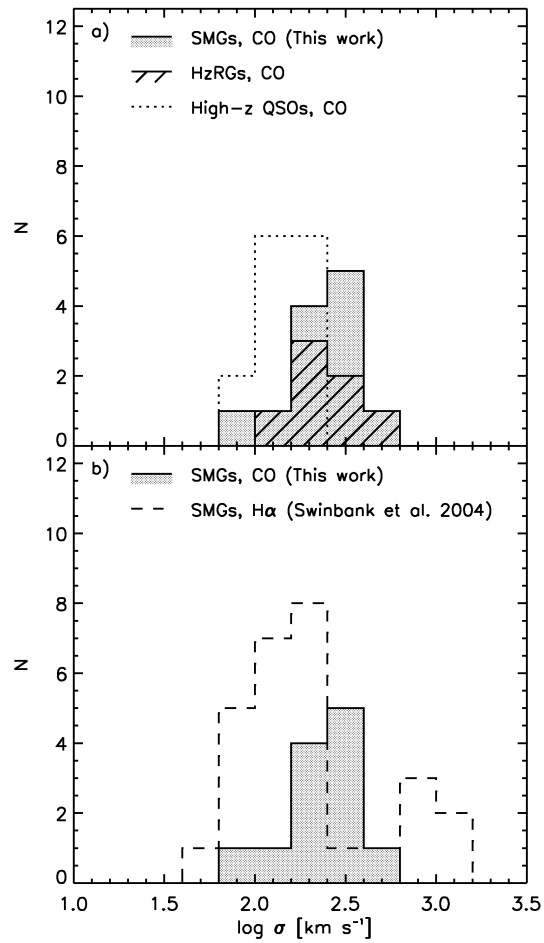


**Figure 6.** (a) Distribution of CO velocity dispersions for high-redshift quasi-sellar objects (QSOs) and high-redshift radio galaxies (HzRGs) from Table 2 and our sample of CO-detected submillimetre galaxies (SMGs). In the cases of the two high-redshift radio galaxies (HzRGs) 4C 60.07 and TN J0924−2201, we have adopted FWHM linewidths of 1000 and $325\,{\rm km\,s^{-1}}$, respectively. In (b), we compare with the measurements of the linewidths of the H$\alpha$ line from near-infrared spectroscopy of a large sample of SMGs (Swinbank et al. 2004).

We now turn to the comparison between SMGs and other high-redshift galaxy populations. Fig. 6(a) compares the distribution of velocity dispersions of our SMG sample with that of all high-redshift QSOs and HzRGs detected in CO to date. While there is a substantial overlap between the SMG and QSO distributions, the latter is seen to peak at somewhat lower velocity dispersions than SMGs and we note that all QSOs have $\log\sigma \leqslant 2.4$ (corresponding to FWHM $\leqslant 590\,{\rm km\,s^{-1}}$). Also, no QSO detected in CO shows evidence of a double-peaked line profile (although a few are spatially resolved, Papadopoulos et al. 2001, Carilli et al. 2002a). A Kolmogorov–Smirnov test suggests that the two distributions are formally different at the 95 per cent confidence level. The apparently lower CO linewidths of QSOs are not clear, although it is possible that they are either intrinsically lower-mass systems or have smaller gas discs. In contrast, there is no discernable difference between the CO linewidths of the SMGs and those HzRGs detected in CO. This suggests that the brightest SMGs have similar dynamical masses and therefore possibly similar dark-matter halo masses to HzRGs, which are believed to be amongst the most massive objects in the high-redshift Universe (inferred from both the presence of a supermassive black hole and the strong clustering of HzRGs, e.g. Ford et al. 1994, Kooiman, Burns & Klypin 1995). However, such a conclusion is uncertain as a result of the small number of objects involved and will have to wait until a larger, more uniform sample of HzRGs has been observed in CO.

In Fig. 6(b), we compare the CO linewidths from our SMG sample with measurements of the width of the H$\alpha$ line from a recent near-infrared spectroscopic survey of 28 SMGs and high-redshift, optically faint, radio-selected starburst galaxies (OFRGs; see e.g. Chapman et al. 2005) by Swinbank et al. (2004). The two distributions span a similar range of velocity dispersions, but the CO sample is skewed towards higher values, resulting in a higher median value. We find that the average ratio between the CO and H$\alpha$ linewidths for SMGs is $\langle{\rm FWHM_{CO}}\rangle/\langle{\rm FWHM_{H\alpha}}\rangle \sim 2$. The main reason for this is likely to be as a result of the CO tracing multiple components in the SMG whereas the long-slit H$\alpha$ spectroscopy is identifying only a single component as a result of the slit orientation or as a result of extreme obscuration in the second component. Part of the discrepancy may also reflect dust obscuration within the galaxy providing only a partial view of the kinematics of the system, in contrast to the obscuration-independent measurement provided by CO. If this

is the case, it could mean that the dynamical masses of SMGs are larger than suggested from their rest-frame optical spectra.

### 5.3 Star formation efficiency and the $L'_{CO}$–$L_{FIR}$ relation

While the luminosity of the CO lines is an indicator of how much molecular gas a galaxy contains, it does not necessarily measure how efficiently this gas is being turned into stars. The star formation efficiency (SFE) can be estimated from the ratio of the far-infrared luminosity of the system to the amount of molecular gas available to form stars, i.e. SFE $= L_{FIR}/M(H_2)$.

The far-infrared luminosities of the SMGs were estimated following Neri et al. (2003), $L_{FIR} = 1.9 \times 10^{12} S_{850}$, where $L_{FIR}$ is in $L_\odot$ and $S_{850}$ in mJy. This assumes a modified greybody model for the far-infrared emission with a dust temperature of $T_d = 40$ K and emissivity $\propto \nu^{1.5}$. The median far-infrared luminosity of the SMG sample is $\langle L_{FIR}\rangle = (1.5 \pm 0.7) \times 10^{13}\,L_\odot$, which is nearly an order of magnitude larger than the most luminous local ULIRGs (SO97). Assuming that the bulk of the far-infrared luminosity is powered by star formation (Frayer et al. 1998; Alexander et al. 2005), we find a median SFE of $\langle \mathrm{SFE}\rangle = 450 \pm 170\,L_\odot\,M_\odot^{-1}$ for the SMG sample, in agreement with the initial findings of Neri et al. (2003). This is somewhat higher than the typical SFE of the local ULIRGs studied by SO97 [$\langle SFE\rangle = 180 \pm 160\,L_\odot\,M_\odot^{-1}$ : using a conversion factor of $X_{CO} = 0.8(\mathrm{K\,km\,s^{-1}\,pc^2})^{-1}\,M_\odot$].

Perhaps a more straightforward measure of the SFE is the continuum-to-line luminosity ratio, $L_{FIR}/L'_{CO}$, because it does not depend on $X_{CO}$. Locally, (U)LIRGs are observed to follow a scaling relation between $L'_{CO}$ and $L_{FIR}$ with the more far-infrared luminous galaxies having proportionally higher CO luminosities (Rickard & Harvey 1984; Young et al. 1984; Sanders & Mirabel 1985; Young et al. 1986). In Fig. 7, we have plotted the SMGs on to the $L'_{CO}$–$L_{FIR}$ diagram along with the (U)LIRGs from our three low-redshift comparison samples. The SMGs extend the general trend seen for the local (U)LIRGs out to far-infrared luminosities $\gtrsim 10^{13}\,L_\odot$. A power-law fit to all three (U)LIRG samples yields $\log L'_{CO} = (0.62 \pm 0.09)\log L_{FIR} + (2.41 \pm 1.06)$. Including the SMGs in the fit yields $\log L'_{CO} = (0.62 \pm 0.08)\log L_{FIR} + (2.33 \pm 0.93)$, i.e. virtually no change in the fit at all. The combined SMG and local ULIRG samples have a statistically significant correlation, as shown by a Spearman's rank-order correlation test, which yields a probability of $P < 0.0001$ that a random (uncorrelated) data set could result in the observed correlation coefficient ($r_S = 0.93$). From Fig. 7, there is even some evidence of an $L'_{CO}$–$L_{FIR}$ correlation within the SMG population itself (the probability of obtaining the observed correlation, $r_S = 0.70$, by chance is $P < 0.0142$). Moreover, the slope of the $L'_{CO}$–$L_{FIR}$ correlation inferred from the fit is significantly less than unity. This is clearly illustrated in Fig. 7 where the locus defined by the data points is seen to have a shallower slope than the line of equality.

The observed slope of the correlation in Fig. 7 implies that the $L_{FIR}/L'_{CO}$ ratio increases with $L_{FIR}$. Several studies have already shown that ULIRGs have higher $L_{FIR}/L'_{CO}$ ratios than the less luminous LIRGs, which in turn have higher ratios than spiral galaxies and giant molecular clouds (GMCs; e.g. Sanders et al. 1986; Solomon & Sage 1988). This trend is shown in Fig. 8 where $L_{FIR}/L'_{CO}$ has been plotted as a function of redshift for the LIRG, ULIRG and SMG samples. The median $L_{FIR}/L'_{CO}$ ratios for LIRGs (Y03) and ULIRGs (SO97) are $50 \pm 30$ and $160 \pm 130\,L_\odot\,(\mathrm{K\,km\,s^{-1}\,pc^2})^{-1}$, respectively. The median far-infrared to CO luminosity ratio for the SMGs is $360 \pm 140\,L_\odot\,(\mathrm{K\,km\,s^{-1}\,pc^2})^{-1}$, which is about a factor of 2 higher than the median value for ULIRGs and suggests that, although some overlap exists between the two populations, in general SMGs have higher star formation efficiencies (SFEs), or a larger contribution to their far-infrared luminosities from a source other than star formation, e.g. an AGN. Although AGN are frequently found in SMGs using extremely deep X-ray observations, these observations also suggest that the AGN are bolometrically insignificant in the vast majority of SMGs (Alexander et al. 2003, 2005).

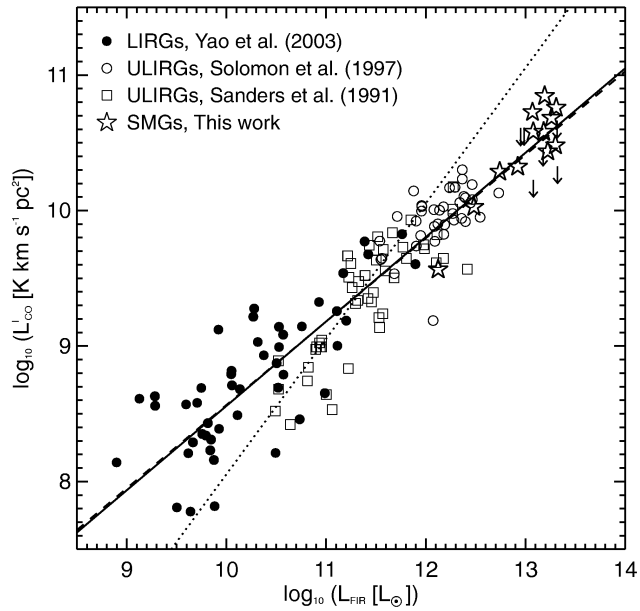


**Figure 7.** A comparison of the CO and far-infrared luminosities ($L'_{CO}$, $L_{FIR}$) for submillimetre galaxies (SMGs) and local ultraluminous infrared galaxies (ULIRGs). As in Fig. 5, the arrows denote the six non-detections. The solid and dashed lines represent fits of the form $\log L'_{CO} = \alpha \log L_{FIR} + \beta$ to all three (ultraluminous) luminous infrared galaxy (LIRG) samples and to the combined (ultraluminous) luminous infrared galaxy (LIRG) and submillimetre galaxy (SMG) samples, respectively. The dotted line is the best fit to all four samples but where the slope has been fixed to unity.

We underline that the above findings are strongly biased towards luminous SMGs, as they are based on a sample of predominantly bright SMGs. This selection effect in conjunction with the CO detection limit of our survey prevent us from probing the lower right portion of Fig. 8, where objects with low $L_{FIR}/L'_{CO}$ ratios reside. It is possible that such objects, which are found locally (see Fig. 8), will also be uncovered at high redshifts by future deep submm and CO observations of a complete sample of high-$z$ starburst galaxies. Intriguingly, however, the $L_{FIR}/L'_{CO}$ ratio of SMM J16359+6612, which has a far-infrared and CO luminosity comparable to the least luminous ULIRGs in the SO97 sample, is higher than almost all the sources in that sample [$360\,L_\odot\,(\mathrm{K\,km\,s^{-1}\,pc^2})^{-1}$].

As a final check, we repeated the above analysis using SMG far-infrared luminosities derived from their radio fluxes and using the radio-FIR correlation (Condon 1992; Yun, Reddy & Condon 2001). There is tentative evidence that this correlation applies out to high redshifts (Garrett 2002; Appleton, Fadda & Marleau 2004) and arguably provides a more reliable estimate of the far-infrared luminosity than that based on the submm flux, which has significant uncertainty associated with it as a result of the unknown dust properties of SMGs. The far-infrared luminosities derived using the radio information are generally larger and the $L'_{CO}$–$L_{FIR}$ correlation therefore shallower ($\alpha = 0.59 \pm 0.08$). In this case, the SMG

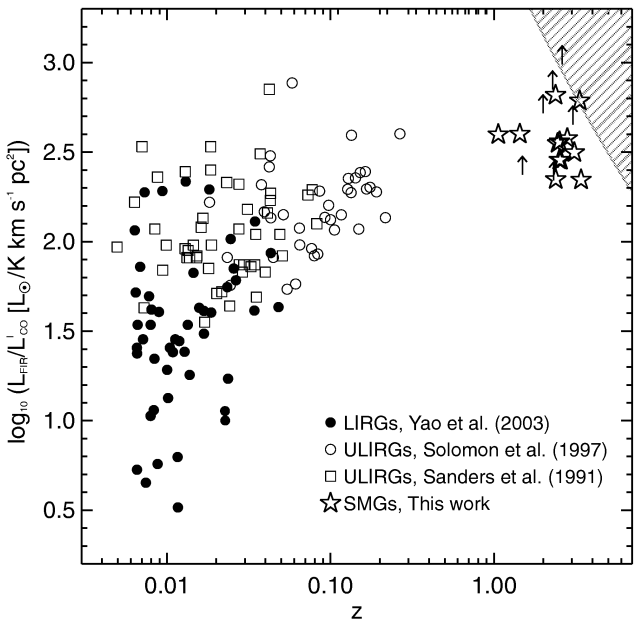


**Figure 8.** The star formation efficiency (SFE) as indicated by the observed ratio $L_{\rm FIR}/L'_{\rm CO}$ as a function of redshifts. Upward pointing arrows represent the six submillimetre galaxies (SMGs) not detected in CO. The hashed region represents the no-detection zone for sources with integrated CO(3–2) fluxes of $I_{\rm CO} \leqslant 0.3\,{\rm Jy\,km\,s^{-1}}$ and submm fluxes of $S_{850\,\mu{\rm m}} \leqslant 4\,{\rm mJy}$.

sample also exhibits a significant correlation, although this can partly be explained by the luminosity distance-squared stretching of the data points.

### 5.4 Discussion

In the previous three subsections, it was found that SMGs have on average 4 times larger CO luminosities, 3–4 times larger linewidths and a median $L_{\rm FIR}/L'_{\rm CO}$ ratio twice that of local ULIRGs. As argued in Section 4.4, the large linewidths and molecular gas masses seen in SMGs are difficult to reconcile with a scenario in which the gas resides in a circumnuclear disc. This is in contrast to what is observed in local ULIRGs where the bulk of the gas is found in an $R \sim 0.5\,{\rm kpc}$ disc or ring. In SMGs, the gas is more likely to be distributed on scales of 2–3 kpc, as suggested by their radio morphologies (Chapman et al. 2004) as well as by high-resolution CO observations of SMGs (Genzel et al. 2003; Tacconi et al. 2005). The typical gas to dynamical mass fraction in SMGs was estimated in Section 4.4 to be $\sim$0.3: almost 2 times higher than the median gas mass fraction in ULIRGs ($\sim$0.16, Downes & Solomon 1998), assuming that the CO–$H_2$ conversion factor is the same for ULIRGs and SMGs. The local gas mass fraction in ULIRGs is measured within the molecular disc ($R \lesssim 0.5\,{\rm kpc}$): however, when averaged over scales of 2–3 kpc, which are the typical scales probed by our CO observations of SMGs, the gas fraction is likely to be significantly smaller. Although, we caution that some of the above arguments are based on a relatively small number of sources detected at a low signal-to-noise ratio or have non-negligible uncertainties associated with them (such as the CO conversion factor), they do seem to suggest, together with the generally higher far-infrared luminosities of SMGs, that the latter are neither high-redshift replicas of local ULIRGs, nor simply scaled-up versions. Rather SMGs appear to more gas-rich and more efficiently star forming than local ULIRGs.

In this respect, it is important to draw attention to observational studies of the depletion of molecular gas with starbursts in ULIRGs. In a sample of more than 50 (U)LIRGs, Gao & Solomon (1999) found a correlation between the CO(1–0) luminosity and the projected separation of the merging nuclei, which they took as evidence for molecular gas being rapidly depleted as a result of intense star formation as the merger progresses. If a similar picture applies at high redshift, the large CO luminosities and gas masses we find for SMGs would imply that these systems are extended and caught in the early stages of merging. However, this might be a premature conclusion because Rigopoulou et al. (1999) did not find any evidence for a correlation between the gas mass and merger phase for local ULIRGs.

If the above trends are verified by future observations, it is interesting to speculate what physical mechanisms could be responsible for the differences between local ULIRGs and SMGs? Both populations appear to result from mergers and strong interactions (e.g. SA91; Chapman et al. 2003c), so what makes the starbursts so much more efficient in SMGs? Numerical simulations have compared the gas flow in major mergers between two galaxies with strong bulges and between two, gas-rich but bulge-less galaxies (Barnes & Hernquist 1996; Iono, Yun & Mihos 2004). In the first case, the gas forms shocked, dense filaments, which dissipate energy and flow towards the centre where they form a nuclear ring that is stabilized by the gravitational potential of the bulge: slowing the rate of star formation. In the second scenario, the merger between two gas-rich but bulge-less galaxies, the gas forms an extended ($\sim$6 kpc), gravitationally significant bar-like structure, which allows the gas to funnel towards the centre. However, without the stabilizing influence of the bulges in the progenitor galaxies, the gas cannot form a stable ring or disc and its density is further increased through the formation of bar-like structures, leading to a wide-spread and vigorous starburst.

These two theoretical scenarios suggest a structural difference between the progenitor galaxies may be at the heart of the differences in behaviour between ULIRGs and SMGs. The suggested structural differences are consistent with the expectations of the typical galaxies involved in mergers at low and high redshifts, with the former involving disc galaxies with significant bulge components (e.g. Lilly et al. 1998), while the progenitor galaxies of SMGs at high redshift are much more likely to be gas-rich, disc-dominated systems with little or no bulge component (Wyse, Gilmore & Franx 1997; Ravindranath et al. 2004). If such structural differences between local and distant starbursts are real, the next question is: at what redshift does the transition occur? In Section 4.3, we found that SMGs at $z \sim 3$ have a higher CO detection rate than SMGs at $z \sim 2$: consistent with the former being more gas-rich. Secondly, the slight preponderance, albeit tentative, of double-peaked CO line profiles at $z \sim 2$ is consistent with that of local ULIRGs and in contrast to SMGs at $z \sim 3$ (see Sections 4.3 and 4.4). Although, these trends are tentative and need a larger survey to confirm or disprove them, together they may indicate a difference in the physical processes responsible for triggering intense star formation in massive galaxies at $z \sim 2$ compared with $z \sim 3$, with major mergers being responsible for much of this activity at lower redshifts (as is the case for local ULIRGs), but a separate mode (requiring less intense perturbations) capable of triggering similar bursts in the more gas-rich systems present at even higher redshifts.

In Section 5.3, we showed that luminous SMGs extend the $L_{\rm CO}$–$L'_{\rm FIR}$ relation of local ULIRGs to higher redshifts and luminosities, and accordingly have higher SFEs than ULIRGs. Although, the SFEs found for the SMGs could be severely overestimated if an AGN contributes significantly to the far-infrared luminosity, the

detection of large amounts of molecular gas in SMGs along with recent X-ray (Alexander et al. 2003, 2005) and radio studies (Chapman et al. 2004) strongly suggest that the bulk of the far-infrared emission from SMGs is powered by a large-scale starburst and not from an AGN. While CO is a good indicator of the total metal-rich $H_2$ gas reservoir, it may be a worse indicator of the amount of dense gas present ($n \geqslant 10^5\,\mathrm{cm}^{-3}$), which actually fuels star formation (Carilli et al. 2005). The latter could be particularly true in the tidally disrupted GMCs expected in ULIRGs, where a diffuse phase may dominate the CO emission but has little to do with star formation (Downes & Solomon 1998; Sakamoto et al. 1999). Such a diffuse phase could be even more pronounced in SMGs with their more extended distributions (Chapman et al. 2003c; Smail et al. 2004). This would explain why the $L_{\rm FIR}/L'_{\rm CO}$ ratio is found to be such a strong function of $L_{\rm FIR}$, increasing for merging systems usually associated with the highest far-infrared luminosities. Interestingly, recent work shows that the SFE of dense gas, parametrized by the $L_{\rm FIR}/L_{\rm HCN(1-0)}$ ratio [the Hydrogen Cyanide (HCN) $J = 1$–0 critical density is $2 \times 10^5\,\mathrm{cm}^{-3}$], remains constant from GMCs all the way to ULIRG system (Gao & Solomon 2003; Solomon et al. 2003; Carilli et al. 2005).

The median star formation rate of the 18 SMGs is $\langle \mathrm{SFR} \rangle \simeq 700\,\mathrm{M}_\odot\,\mathrm{yr}^{-1}$, where we have assumed a Salpeter initial mass function (IMF) and a very conservative limit corresponding to the starburst contributing only 50 per cent of the far-infrared luminosity (see Omont et al. 2001, but cf. Alexander et al. 2005). Our findings in Sections 5.1 and 5.2 have shown that SMGs are massive galaxies with enough molecular gas in them to sustain such a large star formation rate for $\tau_{\rm SMG} \sim M(\mathrm{H}_2)/\mathrm{SFR} \sim 3 \times 10^{10}\,\mathrm{M}_\odot/700\,\mathrm{M}_\odot\,\mathrm{yr}^{-1} \sim 40\,\mathrm{Myr}$. By the end of such a burst, most of the stellar mass corresponding to that of a massive spheroid would be in place. A gas depletion time-scale of $\tau_{\rm SMG} \sim 40\,\mathrm{Myr}$ is comparable to the typical starburst ages ($\sim$ 100–200 Myr) derived from photometric modelling of the broad-band optical/near-infrared colours of SMGs (Smail et al. 2004), although we note that large uncertainties are associated with both methods. For example, the CO observations only probe the gas within the central 10 kpc and as a result the neutral gas, which is likely to be distributed on larger scales, has not been included in our estimate of the gas consumption time-scale. If the H I gas is brought in from $\gtrsim 10\,\mathrm{kpc}$ radius at $\sim 200\,\mathrm{km\,s}^{-1}$, it would reach the central regions in less than 50 Myr, where it could help sustain the vigorous star formation. Furthermore, the above gas consumption time-scale assumes a continuous starburst until all the gas is used: an unlikely scenario because it ignores the negative feedback effects from new-born massive stars and supernovae. For example, one could imagine the starburst terminating prematurely if the gas is removed by starburst- and/or AGN-driven winds only to fall back onto the galaxy at a later stage to fuel a second starburst, thus making the true gas exhaustion time-scale longer. The 40 Myr should therefore be considered a strict lower limit on the starburst phase of SMGs.

An alternative estimate of the duration of the SMG phase can be made from the recent findings by Page et al. (2004) that the 15 per cent of QSOs at $z \sim 2$ that show absorption in their X-ray spectrum are detectable in the submm. Because only 3 per cent of radio-identified SMGs are QSOs (Chapman et al. 2005), this means that SMGs would have a typical lifetime, which is $\sim 0.15/0.03 = 5$ times longer than that of QSOs. Adopting a QSO lifetime of 40 Myr (Martini & Weinberg 2001) yields an SMG life expectancy of $\tau_{\rm SMG} \sim 200\,\mathrm{Myr}$: again larger than the gas consumption time-scale.

If we assume that a large fraction of the gas mass of SMGs is eventually converted into stars (perhaps through repeated cycles of expulsion, infall and star formation), what are the resulting stellar masses of the descendants? Clearly SMGs already contain (perhaps substantial) stellar populations (Smail et al. 2004), however the stellar masses for SMGs are difficult to estimate as a result of significant dust extinction and the resulting uncertainties from the degeneracies between dust reddening and age in evolutionary spectral synthesis models. The best estimates to date, based on *IJK* photometry of 96 SMGs and optically faint μJy radio galaxies (Smail et al. 2004), suggest typical stellar masses of $M_{\rm stars} \simeq 3 \times 10^{10}\,\mathrm{M}_\odot$. Thus, combining the gas and stellar mass estimates, we find that on average SMGs have baryonic masses of $\gtrsim 6 \times 10^{10}\,\mathrm{M}_\odot$, which is comparable to the masses of local early-type $L^*$ galaxies.

The discussion above suggests that SMGs are in fact the progenitors of massive spheroids in the present-day Universe and that the build-up of the stellar population occurs rapidly ($40 \lesssim \tau_{\rm SMG} \lesssim 100\,\mathrm{Myr}$), consistent with the old homogeneous stellar populations of local ellipticals. Further evidence in support of this is (i) the strong clustering claimed for SMGs (Blain et al. 2004b) and (ii) the fact that the rest-frame optical properties of SMGs match the bright end of the luminosity function of spheroidal galaxies in nearby clusters (Smail et al. 2004).

## 6 IMPLICATIONS FOR STRUCTURE-FORMATION MODELS

Semi-analytical models of galaxy formation and evolution (Cole et al. 1994; Kauffmann et al. 1999; Cole et al. 2000; Somerville, Primack & Faber 2001) have enjoyed a fair degree of success in reproducing the properties of galaxies in the local Universe, e.g. the luminosity function, the distribution of colours and disc scalelengths of galaxies, the observed mix of morphologies and the Tully–Fisher relation (e.g. Kauffmann et al. 1999; Cole et al. 2000). However, the key observable with which to benchmark models of galaxy formation and evolution is the mass assembly of galaxies, and in particular the assembly of baryonic mass, as a function of redshift.

Genzel et al. (2003) pointed out that, if the extremely large baryonic mass ($\gtrsim 10^{11}\,\mathrm{M}_\odot$) of SMM J02399−0136 was representative of the bright SMG population, then the high surface density of such sources would imply that the abundance of very massive baryonic systems at high redshift was about an order of magnitude larger than predicted by semi-analytical models (see also Tecza et al. 2004).

Here, we repeat this analysis using the 10 SMGs in our sample, which lie in the redshift range $z = 2$–3.5 and have reliable gas mass estimates, to put lower limits on the comoving number density of massive galaxies at high redshifts. The redshift interval considered translates into $\sim 1.5\,\mathrm{Gyr}$ in terms of elapsed cosmic time and corresponds to a comoving volume of $1.8 \times 10^7\,\mathrm{Mpc}^3\,\mathrm{deg}^{-2}$. The average submm flux of the 10 SMGs is $\langle S_{850\,\mu\mathrm{m}} \rangle = 8 \pm 4\,\mathrm{mJy}$. The surface density on the sky of SMGs with fluxes $\gtrsim 8\,\mathrm{mJy}$ is $285^{+231}_{-149}\,\mathrm{deg}^{-2}$ (Borys et al. 2003). Taking into account that (i) approximately 60 per cent of the bright SMG population lie within $z = 2$–3.5 (Chapman et al. 2003b, 2005) and (ii) the CO detection fraction of SMGs in the redshift range $2 \leqslant z \leqslant 3.5$ is 10/14 ($\sim$ 71 per cent), we estimate that the comoving number density of galaxies with baryonic masses $\gtrsim 6 \times 10^{10}\,\mathrm{M}_\odot$ in the redshift interval $z = 2$–3.5 is $\sim 5.1^{+7.6}_{-3.4} \times 10^{-6}\,\mathrm{Mpc}^{-3}$. The errors are estimated by propagating the $1\sigma$ limits on the submm flux and number counts through the same calculation.

Because we only observe SMGs during their submm-luminous phase, we have to correct the derived space density by a factor corresponding to the ratio between the 1.5 Gyr, which has elapsed over the redshift range $z = 2.0$–3.5, and the typical duration of the SMG phase. The latter is uncertain, but as we saw in

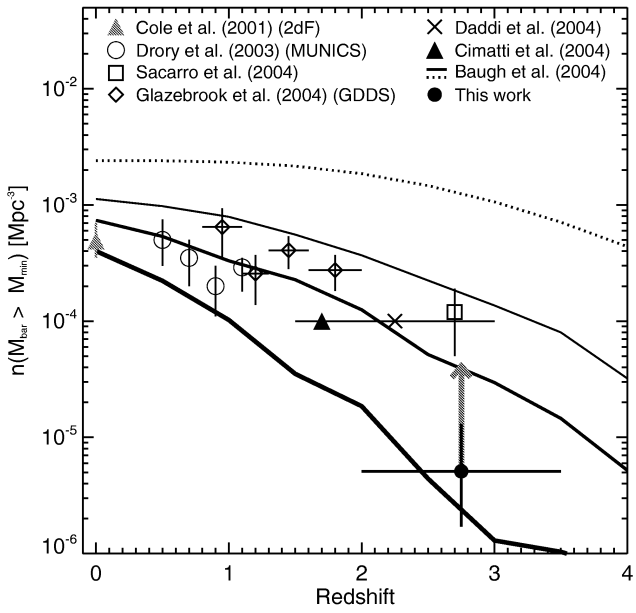


**Figure 9.** The comoving number density of galaxies with baryonic masses $\sim 6 \times 10^{10}\,M_\odot$ as derived from CO observations of submillimetre galaxies (SMGs). The GALFORM model (Cole et al. 2001; Baugh et al. 2005) predictions of the abundances of galaxies with baryonic masses $\geqslant 5$, 7 and $10 \times 10^{10}\,M_\odot$ as a function of redshift are shown as thin, medium and thick solid lines, respectively. The dotted curve represents the total baryonic matter content available in $\geqslant 10^{11}\,M_\odot$ dark matter haloes and is obtained by scaling the abundance of haloes with the cosmological baryon-to-dark matter density ($\Omega_b/\Omega_{DM} = 0.13$). This provides a strict upper limit on the number density of massive baryonic galaxies at a given redshift. The observations can be reconciled within the cold dark matter (CDM) framework, provided that $\sim 10$ per cent of all baryons within dark matter haloes are rapidly assembled into galaxies.

Section 5.4 it is likely to lie in the range 40–200 Myr. Adopting 200 Myr as a conservative upper value for the submm luminous phase, we estimate a correction factor of $\sim 8$.

In Fig. 9, we have plotted our estimate of the comoving number density of $\gtrsim 6 \times 10^{10}\,M_\odot$ systems at $z \sim 2.8$ and the (conservative) correction factor that must be applied. Our estimate of the abundances of massive galaxies at $z \sim 2.8$ is in good agreement with independent measurements at similar redshifts (Daddi, Cimatti & Renzini 2004; Saracco et al. 2004) and confirms the slow decline in the space density of massive galaxies as a function of redshift (Genzel et al. 2003; Glazebrook et al. 2004).

The abundance tracks of $\geqslant 5 \times 10^{10}$ and $\geqslant 7 \times 10^{10}\,M_\odot$ systems as predicted by the most recent semi-analytic models such as GALFORM (Cole et al. 2001; Baugh et al. 2005) are seen to envelope our estimated volume density. There are two reasons for the closer agreement between the observations and models than previous work: (i) the typical baryonic mass of bright SMGs is not 2–3 $m^*$ but rather $\sim 0.6\,m^*$ and (ii) the new GALFORM model, which employs a top-heavy IMF in order to account for the 850-μm number counts (Baugh et al. 2005), also predicts higher abundances of massive galaxies at high redshifts than previous models. Other semi-analytical models (Fontana, Pozzetti & Donnarumma 2004; Granato et al. 2004) have also modified their recipes so that their models fit the data.

We stress, however, that by using an SMG time-scale of 200 Myr and not 40 Myr as suggested by the CO observations, our estimate of the correction factor is a conservative one. Furthermore, if the population of OFRGs, whose faint levels of submm flux are believed to be a result of their higher dust temperatures (Blain et al. 2004a; Chapman et al. 2005), have similar gas masses to classical SMGs (Smail et al. 2004; Swinbank et al. 2004), this would double our current estimate of the abundance of massive baryonic galaxies at high redshifts.

We conclude that, given the small number of sources and crude redshift bins used in our calculations and the large uncertainty on the correction factors that have to be applied, there is no evidence for a severe discrepancy between observations and the latest theoretical predictions. An increase in our sample size would not only allow us to confirm this but also would allow us to split the sample into mass bins and compare with different mass track predictions.

## 7 CONCLUSIONS

We present results from a PdBI CO Survey of SMGs with radio counterparts. We successfully detect CO in four out of 10 SMGs observed, which brings the total number of SMGs detected by our survey to seven out of 13 observed. In addition, we have also presented a detection of CO based on archival observations of SMM J02396−0134. Combining these 14 sources with four CO-detected SMGs from the literature, we have compiled a sample of 18 SMGs observed in CO of which 12 are detected. We use this unique sample to derive the bulk gas properties and masses of the most luminous SMGs.

(i) We find that the SMGs in our sample have a median CO luminosity of $\langle L'_{CO}\rangle = (3.8 \pm 2.0) \times 10^{10}\,K\,km\,s^{-1}\,pc^2$. This corresponds to a molecular gas mass of $\langle M(H_2)\rangle = (3.0 \pm 1.6) \times 10^{10}\,M_\odot$ (within $R \lesssim 2$ kpc), assuming a conversion factor of $X_{CO} = 0.8(K\,km\,s^{-1}\,pc^2)^{-1}\,M_\odot$ and optically thick, thermalized line ratios. Although considerable uncertainty is associated with $X_{CO}$, it is clear that bright SMGs are amongst the most gas-rich systems in the Universe. Comparing with local ULIRGs, we find that SMGs have molecular gas reservoirs on average about 4 times greater than even the most CO-luminous ULIRGs. We argue that this is largely a result of the evolution in the molecular gas content of the most far-infrared luminous galaxies with redshift.

(ii) In general, the SMGs in our sample have extremely broad line profiles. The median FWHM is $780 \pm 320\,km\,s^{-1}$, which is $\gtrsim 3$ times larger than the average CO(1–0) linewidth of local ULIRGs. The large linewidths and in some cases multiple-peaked CO spectra, together with the vast amounts of molecular gas, suggests that the brightest SMGs are merger events. We argue that the observed gas properties are difficult to reconcile with the scenario witnessed in local ULIRGs where the bulk of the molecular gas resides in a compact circumnuclear disc.

(iii) We find that the median dynamical mass of the SMG sample is $\langle M_{dyn}\rangle = (1.2 \pm 1.5) \times 10^{11}\,M_\odot$ within the central $\sim$4 kpc. This suggests that the brightest SMGs are amongst the most massive galaxies in the distant Universe, comparable in mass to the most extreme HzRGs and QSOs, rather than being high-$z$ replicas of local ULIRGs. Taking into account the stellar mass component, we estimate that the total baryonic mass content of SMGs is $\gtrsim 6 \times 10^{10}\,M_\odot$. Thus we conclude that not only are SMGs very massive baryonic systems, but the baryons can account for a substantial fraction of the total mass in the central regions.

(iv) We have shown that the SMGs exhibit a non-linear correlation between far-infrared and CO luminosity, similar to that observed for local ULIRGs. This not only extends the $L'_{CO}$–$L_{FIR}$ relation to

higher luminosities ($L_{\rm FIR} \sim 10^{12-14}\,{\rm L}_{\odot}$), but also shows that it holds at the highest redshifts. The main implication of this is that SMGs have higher $L_{\rm FIR}/L'_{\rm CO}$ ratios than ULIRGs and therefore possibly higher SFEs. However, a clearer picture of the SFE of SMGs has to await a future systematic survey for high-redshift HCN, which will trace the dense star-forming gas.

(v) From the inferred molecular gas masses, we estimate a typical gas consumption time-scale of $\gtrsim 40$ Myr. Given the large uncertainties involved, an SMG phase of $\sim 40$ Myr is roughly consistent with the best age estimates of the starbursts in SMGs (Smail et al. 2003, 2004; Tecza et al. 2004), which in turn agree favourably with independent estimates of the duration of the SMG phase obtained by requiring a scenario in which SMGs last 100–200 Myr before going through an ∼10 Myr QSO phase at $z \sim 2$, becoming massive evolved galaxies at $z \sim 1$, followed by a period of passive evolution that sees them ending up as old $\gtrsim L^*$ ellipticals in the present day. Furthermore, the slightly short gas consumption time-scales can easily be prolonged by invoking negative feedback processes and may be indicative of such processes playing an important role in the build-up of massive galaxies.

(vi) From our observations, we place a lower limit on the comoving number density of massive baryonic systems in the redshift range $z = 2$–$3.5$ of $n(M_{\rm bar} \geqslant 6 \times 10^{10}\,{\rm M}_{\odot}) \gtrsim 5.1 \times 10^{-6}\,{\rm Mpc}^{-3}$ in agreement with results from recent near-infrared/spectroscopic surveys (e.g. Glazebrook et al. 2004; Saracco et al. 2004). Given the substantial uncertainties involved, we find no significant discrepancy between the data and the predicted abundances of massive galaxies at high redshifts.

## ACKNOWLEDGMENTS

TRG acknowledges support from the Danish Research Council and from the European Union RTN network, POE. IS acknowledges support from the Royal Society. AWB acknowledges support from NSF grant AST-0205937, from the Research Corporation and the Alfred P. Sloan Foundation. JPK thanks Caltech and CNRS for support. We are grateful to Genevieve Soucail and Paola Andreani for letting us use the PdBI CO data for SMM J02396−0134 and ERO J16540+4626, respectively. We also thank Cedric Lacey for providing the GALFORM model predictions. Finally, we thank Dennis Downes for useful comments and suggestions and for allowing us to reproduce the PdBI CO data for SMM J14011+0252.

## REFERENCES

Aalto S., Booth R. S., Black J. H., Johansson L. E. B., 1995, A&A, 300, 369
Adelberger K. L., Steidel C. C., 2000, ApJ, 544, 218
Alexander D. M. et al., 2003, AJ, 126, 539
Alexander D. M., Bauer F. E., Chapman S. C., Smail I., Blain A. W., Brandt W. N., Ivison R. J., 2005, in Bender R., Renzini A., eds, Proc. ESO Workshop, Multiwavelength Mapping of Galaxy Formation and Evolution, Springer, Berlin, in press (astro-ph/0401129)
Alloin D., Barvainis R., Guilloteau S., 2000, ApJ, 528, L81
Andreani P., Casoli F., Gerin M., 1995, A&A, 300, 43
Andreani P., Cimatti A., Loinard L., Röttgering H., 2000, A&A, 354, L1
Appleton P. N., Fadda S. T., Marleau F. R., 2004, ApJS, 154, 147
Baker A. J., Tacconi L. J., Genzel R., Lehnert M. D., Lutz D., 2004, ApJ, 604, 125
Barger A. J., Cowie L. L., Sanders D. B., 1999, ApJ, 518, L5
Barnes J. E., Hernquist L., 1996, ApJ, 471, 115
Barvainis R., Tacconi L., Antonucci R., Alloin D., Coleman P., 1994, Nat, 371, 586
Barvainis R., Maloney P., Antonucci R., Alloin D., 1997, ApJ, 484, 695
Barvainis R., Alloin D., Guilloteau S., Antonucci R., 1998, ApJ, 492, L13
Barvainis R., Alloin D., Bremer M., 2002, A&A, 385, 399
Baugh C. M., Lacey C. G., Frenk C. S., Granato G. L., Silva L., Bressan A., Benson A. J., Cole S., 2005, MNRAS, 356, 1191
Beelen A. et al., 2004, A&A,423, 441
Bertoldi F., Menten K. M., Kreysa E., Carilli C. L., Owen F., 2000, in 24th Meeting of the IAU, Joint Discussion 9, Manchester
Bertoldi F. et al., 2003, A&A, 409, L47
Binney J., Tremain S., 1987, Galactic Dynamics. Princeton Univ. Press Princeton
Blain A. W., Jameson A., Smail I., Longair M. S., Kneib J.-P., Ivison R. J., 1999, MNRAS, 309, 715
Blain A. W., Smail I., Ivison R. J., Kneib J.-P., Frayer D. T., 2002, Phys. Rep., 369, 111
Blain A. W., Chapman S. C., Smail I., Ivison R. J., 2004a, ApJ, 611, 52
Blain A. W., Chapman S. C., Smail I., Ivison R. J., 2004b, ApJ, 611, 725
Borys C., Chapman S. C., Halpern M., Scott D., 2003, MNRAS, 344, 385
Braine J., Combes F., 1992, A&A, 264, 433
Brown R. L., Vanden Bout P. A., 1991, AJ, 102, 1956
Carilli C. L. et al., 2002a, AJ, 123, 1838
Carilli C. L. et al., 2002b, ApJ, 575, 145
Carilli C. L. et al., 2005, ApJ, in press (astro-ph/0409054)
Chapman S. C. et al., 2003a, ApJ, 585, 57
Chapman S. C., Blain A. W., Ivison R. J., Smail I., 2003b, Nat, 422, 695
Chapman S. C., Windhorst R., Odewahn S., Yan H., Conselice C. J., 2003c, ApJ, 599, 92
Chapman S. C., Smail I., Windhorst R., Muxlow T., Ivison R. J., 2004, ApJ, 611, 732
Chapman S. C., Blain A. W., Ivison R. J., Smail I., 2005, ApJ, 622, 772
Cimatti A., Andreani P., Röttgering H., Tilanus R., 1998, Nat, 392, 895
Cimatti A. et al., 2004, Nat, 430, 184
Cole S., Aragon-Salamanca A., Frenk C. S., Navarro J. F., Zepf S. E., 1994, MNRAS, 271, 781
Cole S., Lacey C. G., Baugh C. M., Frenk C. S., 2000, MNRAS, 319, 168
Cole S. et al., 2001, MNRAS, 326, 255
Condon J. J., 1992, ARA&A, 30, 575
Cox P. et al., 2002, A&A, 387, 406
Daddi E., Cimatti A., Renzini A., 2004, ApJ, 600, L127
De Breuck C. et al., 2003a, A&A, 401, 911
De Breuck C., Neri R., Omont A., 2003b, New Astron. Rev., 47, 285
De Breuck C., Downes D., Neri R., van Breugel W., Reuland M., Omont A., Ivison R., 2005, A&A, 430, L1
Devereux N., Taniguchi Y., Sanders D. B., Nakai N., Young J. S., 1994, AJ, 107, 2006
Dey A., Graham J. R., Ivison R. J., Smail I., Wright G. S., Liu M. C., 1999, ApJ, 519, 610
Downes D., Solomon P. M., 1998, ApJ, 507, 615
Downes D., Solomon P. M., 2003, ApJ, 582, 37
Downes D., Solomon P. M., Radford S. J. E., 1995, ApJ, 453, L65
Downes D., Neri R., Wiklind T., Wilner D. J., Shaver, P. A., 1999, ApJ, 513, L1
Drory N., Bender R., Snigula J., Feulner, G., Hopp, U., Maraston C., Hill G. J., Mendes de Oliveira C., 2003, in Bender R., Renzini A., eds, Proc. ESO/USM Workshop, The Mass of Galaxies at Low and High Redshift. Springer, Berlin (astro-ph/0201207), p. 140
Dunne L., Eales S., Edmunds M., Ivison R. J., Alexander P., Clements D. L., 2000, MNRAS, 315, 115
Fontana A., Pozzetti L., Donnarumma I., 2004, A&A, 424, 23
Ford H. C. et al., 1994, ApJ, 435, L27
Frayer D. T., Ivison R. J., Scoville N. Z., Yun M., Evans A. S., Smail I., Blain A. W., Kneib J.-P., 1998, ApJ, 506, L7
Frayer D. T. et al., 1999, ApJ, 514, L13
Frayer D. T., Armus L., Scoville N. Z., Blain A. W., Reddy N. A., Ivison R. J., Smail Ian, 2003, ApJ, 126, 73
Gao Y., Solomon P. M., 1999, ApJ, 512, L99
Gao Y., Solomon P. M., 2003, ApJ, 606, 271
Garrett M. A., 2002, A&A, 384, L19
Genzel R., Baker A. J., Tacconi L. J., Lutz D., Cox P., Guilloteau S., Omont A., 2003, ApJ, 584, 633

Glazebrook K. et al., 2004, Nat, 430, 181
Granato G. L., De Zotti G., Silva L., Bressan A., Danese, L., 2004, ApJ, 600, 580
Greve T. R., Ivison R. J., Papadopoulos P. P., 2003, ApJ, 599, 839
Greve T. R., Ivison R. J., Papadopoulos P. P., 2004a, A&A, 419, 99
Greve T. R., Ivison R. J., Bertoldi F., Stevens J. A., Dunlop J. S., Lutz D., Carilli C. L., 2004b, MNRAS, 354, 779
Guilloteau S., Lucas R., 2000, in Magnum J. G., Radford S. J. E., eds, ASP Conf. Ser. Vol. 217, Imaging at Radio through Submillimeter Wavelengths. Astron. Soc. Pac., San Francisco, p. 299
Guilloteau S., Omont A., McMahon R. G., Cox P., Petitjean P., 1997, A&A, 328, L1
Guilloteau S., Omont A., Cox P., McMahon R. G., Petitjean P., 1999, A&A, 349, 363
Hainline L. J., Scoville N. Z., Yun M. S., Hawkins D. W., Frayer D. T., Isaak K. G., 2004, ApJ, 609, 61
Holland W. S. et al., 1999, MNRAS, 303, 659
Hu E. M., Ridgway S. E., 1994, AJ, 107, 1303
Iono D., Yun M. S., Mihos J. C., 2004, ApJ, 616, 199
Ivison R. J., Smail I., Barger A. J., Kneib J.-P., Blain A. W., Owen F. N., Kerr T. H., Cowie L. L., 2000, MNRAS, 315, 209
Ivison R. J., Smail I., Frayer D. T., Kneib J.-P., Blain A. W., 2001, ApJ, 561, L45
Ivison R. J. et al., 2002, MNRAS, 337, 1
Kauffmann G., Colberg J. M., Diaferio A., White S. D. M., 1999, MNRAS, 303, 188
Klamer I. J., Ekers R. D., Sadler E. M., Weiss A., Hunstead R. W., De Breuck C., 2005, ApJ, 612, L1
Kneib J.-P., Neri R., Smail I., Blain A. W., Sheth K., van der Werf P., Knudsen K. K., 2004, A&A, 614, L5
Knudsen K. K., van der Werf P. P., Jaffe W., 2003, A&A, 411, 343
Kooiman B. L., Burns J. O., Klypin A. A., 1995, ApJ, 448, 500
Kreysa E. et al., 1998, SPIE, 3357, 319
Krips M., Neri R., Eckart A., Martin-Pintado J., Planesas P., Colina L., 2004, in Pfalzner S., Kramer C., Straubmeier C., Heithausen A., eds, Proc. 4th Cologne-Bonn-Zermatt-Symposium. Springer Verlag, Berlin, Vol. 91, p. 23
Ledlow M. J., Smail Ian, Owen F. N., Keel W. C., Ivison R. J., Morrison G. E., 2002, ApJ, 577, L79
Lewis G. F., Carilli C. L., Papadopoulos P. P., Ivison R. J., 2002, MNRAS, 330, L15
Lilly S. et al., 1998, ApJ, 500, L75
Martini P., Weinberg D. H., 2001, ApJ, 547, 12
Mirabel I. F., Sanders D. B., 1989, ApJ, 340, L53
Neri R. et al., 2003, ApJ, 597, L113
Ohta K., Yamada T., Nakanishi K., Kohno K., Akiyama M., Kawabe R., 1996, Nat, 382, 426
Oke J. B. et al., 1995, PASP, 107, 375
Omont A., Petitjean P., Guilloteau S., McMahon R. G., Solomon P. M., Pecontal E., 1996, Nat, 382, 428
Omont A., Cox P., Bertoldi F., McMahon R. G., Carilli C., Isaak K. G., 2001, A&A, 374, 371
Page M., Stevens J. A., Ivison R. J., Carrera F. J., 2004, ApJ, 611, L85
Papadopoulos P. P., Ivison R. J., 2002, ApJ, 564, L9
Papadopoulos P. P., Röttgering H. J. A., van der Werf P. P., Guilloteau S., Omont A., Breugel W. J. M., Tilanus R. P. J., 2000, ApJ, 528, 626
Papadopoulos P. P., Ivison R. J., Carilli C. L., Geraint L., 2001, Nat, 409, 58
Planesas P., Martin-Pintado J., Neri R., Colina L., 1999, Sci, 286, 2493
Ravindranath S. et al., 2004, ApJ, 604, L9
Richards G. T., Vanden Berk D. E., Reichard T. A., Hall P. B., Schneider D. P., SubbaRao M., Thakar A. R., York D. G., 2002, AJ, 124, 1
Rickard L. J., Harvey P. M., 1984, AJ, 89, 1520
Rickard L. J., Palmer P., Morris M., Turner B. E., Zuckerman B., 1975, ApJ, 199, L75
Rigopoulou D., Spoon H. W. W., Genzel R., Lutz D., Moorwood A. F. M., Tran Q. D., 1999, AJ, 118, 2625
Sakamoto K., Scoville N. Z., Yun M. S., Crosas M., Genzel R., Tacconi L. J., 1999, ApJ, 514, 68
Sanders D. B., Mirabel I. F., 1985, ApJ, 298, L31
Sanders D. B., Scoville N. Z., Young J. S., Soifer B. T., Schloerb F. P., Rice W. L., Danielson G. E., 1986, ApJ, 305, L49
Sanders D. B., Scovillle N. Z., Soifer B. T., 1991, ApJ, 370, 158 (SA91)
Saracco P. et al., 2004, A&A, 420, 125
Scott S. E. et al., 2002, MNRAS, 331, 817
Scoville N. Z., Yun M. S., Windhorst R. A., Keel W. C., Armus L., 1997, ApJ, 485, L21
Seaquist E. R., Ivison R. J., Hall P. J., 1995, MNRAS, 276, 867
Sheth K., Blain A. W., Kneib J.-P., Frayer D. T., van der Werf P., Knudsen K. K., 2004, ApJ, 614, L5
Simpson C., Dunlop J. S., Eales S. A., Ivison R. J., Scott S. E., Lilly S. J., Webb T. M. A., 2004, MNRAS, 353, 179
Smail I., Ivison R. J., Blain A. W., 1997, ApJ, 490, L5
Smail I., Ivison R. J., Kneib J.-P., Cowie L. L., Blain A. W., Barger A. J., Owen F. N., Morrison, G., 1999, MNRAS, 308, 1061
Smail I., Ivison R. J., Blain A. W., Kneib J.-P., 2002, MNRAS, 331, 495
Smail I., Chapman S. C., Ivison R. J., Blain A. W., Takata T., Heckman T. M., Dunlop J. S., Sekiguchi K., 2003, MNRAS, 342, 1185
Smail I., Chapman S. C., Blain A. W., Ivison R. J., 2004, ApJ, 616, 71
Solomon P. M., Sage L. J., 1988, ApJ, 334, 613
Solomon P. M., Downes D., Radford S. J. E., 1992a, Nat, 356, 318
Solomon P. M., Downes D., Radford S. J. E., 1992b, ApJ, 398, L29
Solomon P. M., Downes D., Radford S. J. E., Barrett J. W., 1997, 478, 144 (SO97)
Solomon P. M., Vanden Bout P., Carilli C. L., Guelin M., 2003, Nat, 426, 636
Somerville R. S., Primack J. R., Faber S. M., 2001, MNRAS, 320, 504
Soucail G., Kneib J.-P., Bezecourt J., Metcalfe L., Altieri B., Le Borgne J. F., 1999, A&A, 343, L70
Spergel D. N. et al., 2003, ApJS, 148, 175
Swinbank A. M., Smail I., Chapman S. C., Blain A. W., Ivison R. J., Keel W. C., 2004, ApJ, 617, 64
Swinbank A. M. et al., 2005, MNRAS, in press (doi:10.1111/j.1365-2966.2005.08901.x)
Tacconi L. et al., 2005, ApJ, submitted
Tecza M. et al., 2004, ApJ, 604, L109
Walter F. et al., 2003, Nat, 424, 406
Webb T. M. et al., 2003, ApJ, 587, 41
Weiss A., Henkel C., Downes D., Walter F., 2003, A&A, 409, L41
White S. D. M., Frenk C. S., 1991, ApJ, 379, 52
Wilner D. J., Zhao J.-H., Ho P. T. P., 1995, ApJ, 453, L91
Wyse R. F. G., Gilmore G., Franx M., 1997, ARA&A, 35, 637
Yao L., Seaquist E. R., Kuno N., Dunne L., 2003, ApJ, 588, 771 (Y03)
Young J. S., Kenney J., Lord S. D., Schloerb F. P., 1984, ApJ, 287, L65
Young J. S., Schloerb F. P., Kenney J. D., Lord S. D., 1986, ApJ, 304, 443
Yun M. S., Reddy N. A., Condon J. J., 2001, ApJ, 554, 803

This paper has been typeset from a TEX/LATEX file prepared by the author.